2008

DYNAMIC MODELS FOR INDUCTION CHARGING OF SPHERICAL PARTICLES WITH SURFACE CONDUCTIVITY

Bassem F. Nader
Western University

DYNAMIC MODELS FOR INDUCTION CHARGING OF SPHERICAL PARTICLES WITH SURFACE CONDUCTIVITY

(Spine title: Induction Charging of Particles with Surface Conductivity)

(Thesis format: Monograph)

by

Bassem F. Nader

Graduate Program in Engineering Science
Department of Electrical and Computer Engineering

A thesis submitted in partial fulfillment
of the requirements for the degree of
Master of Engineering Science

School of Graduate and Postdoctoral Studies
The University of Western Ontario
London, Ontario, Canada

THE UNIVERSITY OF WESTERN ONTARIO
SCHOOL OF GRADUATE AND POSTDOCTORAL STUDIES

CERTIFICATE OF EXAMINATION

Supervisor

Dr. K. Adamiak

Co-Supervisor

Dr. G.S.P. Castle

Supervisory Committee

Examiners

Dr. W. Greason

Dr. A. Dounavis

Dr. J. Yang

The thesis by

Bassem F. Nader

entitled:

Dynamic Models for Induction Charging of Spherical Particles with Surface Conductivity

is accepted in partial fulfilment of the
requirements for the degree of
Master of Engineering Science

Date _____

Chair of the Thesis Examination Board

Abstract

The purpose of this research was to investigate the dynamics of induction charging for spherical particles assuming finite volume and surface conductivities, and arbitrary particle permittivity. All results, presented in this thesis, were based on numerical simulations on the COMSOL commercial software using the Finite Element Method. Simulations were performed for a conducting spherical particle with finite surface conductivity. The particle was resting on a ground electrode and exposed to an external electric field. The model was then extended to investigate multiple spherical particles stacked in an arbitrary pattern structure. Saturation charge and actual charging time constant were investigated. The rate of charge accumulation was affected significantly by the particle's volume and surface conductivities, contact area with the ground electrode, and electric shielding due to proximity of stacked particles. To a less extent, the actual charging time was affected by particle permittivity. Furthermore, shielding the electric field from a given particle reduced its saturation charge significantly.

Keywords: Induction charge, surface conductivity, spherical particle, charging time constant, relaxation time constant, electric field, electric shielding, surface charge density, finite element method, conductivity, permittivity.

Dedicated to
My Dear Father and Mother
Dunia and her family
and Elias and his family

Thank you...

Acknowledgements

A significant appreciation goes to my supervisors Dr. K. Adamiak and Dr. G.S.P. Castle for their wisdom and support throughout my graduate studies. This research work was perfectly conducted because of their relentless support. They have been my mentors to the utmost degree, guiding me in the right direction every step of the way and paving my academic pursuit.

I would also like to thank Dr. Shahwan Khoury, my professor in undergraduate studies, who has helped me get to this stage and follow this research field.

A special thank you must go to Christine Bonatsos, a one of a kind person and close friend, who has been there for me unconditionally during the good and bad times.

Appreciation and deepest gratitude are extended to my best friends Tony, Naji, Elie, Karim, and Jad for the unlimited support they have shown to finish this work.

I would like to dedicate a special thank you for my father Faisal Nader; I owe him what I am today. He has relentlessly pushed me to achieve the best results in my academics.

Last but not least, my wholehearted appreciation, gratitude and love to my family, my parents Faisal and Siham, brother Elias and his family, and sister Dunia and her family for their endless love and support during my study. To them I dedicate this thesis.

Table of Contents

List of Tables

List of Figures

Nomenclature

Symbol	Description	Unit
a	radius of inner sphere	mm
b	radius of outer sphere	mm
d	surface layer thickness of particle	mm, Å
$\vec{D}$	electrostatic displacement vector	C/m²
D_n	normal component of electrostatic displacement vector	C/m²
$\vec{E}$	electric field vector	V/m
E_0	uniform applied external electric field	V/m
E_t	tangential component of the electric field vector	V/m
$\vec{j}$	current density vector	A/m²
J_n	normal current density flow into the surface of the particle	A/m²
Q	induction charge	C
Q_s	saturation charge for a particle	C
R	resistor	ohms
C	capacitor	F
S	contact area of the particle with ground electrode	mm²
t	time	s
t_{sa}	saturation charging time	s

V_0	DC voltage applied to the upper electrode	V
ε	permittivity	F/m
ε_0	permittivity of vaccuum	F/m
ε_r	relative permittivity	
Φ	electrostatic potential	V
ρ	space charge density	C/m^3
ρ_s	surface charge density	C/m^2
σ	volume conductivity	S/m
σ_s	surface conductivity	S/square
τ_c	actual charging time constant	s
τ_d	actual discharging time constant	s
τ_r	material relaxation time constant	s

Chapter 1
Introduction

1.1 Introduction

Many electrostatic applications rely on electric charging of particles. Electrostatic separation, precipitation and powder coating are examples of common processes that use electric charging. Among different charging mechanisms, induction charging is often preferred as it can be easily controlled and it doesn't require ambient gas ionization.

In the most typical case, induction charging can be achieved by grounding an electrically conducting or semi-conducting object and exposing it to an electric field. Initially, electric charges will move inside the conducting object, as the electric current flows through the material, and accumulate on the conducting surface. The charges will only be distributed on the surface of the conducting or semi-conducting object with a zero net induced charge inside. After some time the electric field of induced charges completely cancels the external electric field, current flow stops and the steady-state is reached. The total electric charge accumulated on the particle surface is called the saturation charge. "For an ideal insulator induction charging is not possible since the charges cannot move within the material" [4].

This thesis presents the results of investigations of the induction charging of spherical particles made out of real conductors with arbitrary permittivity and finite volume and surface conductivities. In practical applications, particles are arbitrary in shape. For analysis purposes, only spherical particles have been considered. This is

because the charging level of particles can be predicted analytically only for highly symmetrical particle shapes.

Analytical methods can be used to evaluate the charging level of some regularly shaped particles, such as spheres and hemispheres [2]. Analytical results can be used to validate the algorithms and models for numerical simulation. The numerical models can then be modified to include other factors that affect the accumulation of charge (shape, material properties), and to study the dynamics of the charge build-up. The results presented in literature so far are valid for uniformly conductive particles only. Little research has been done to show the effect of the surface conductivity, which can be important in some applications. In some cases, the term surface resistivity is used and is inversely proportional to surface conductivity. "Surface resistivity is the resistance to leakage current along the surface of an insulating material. Volume resistivity is the resistance to leakage current through the body of an insulating material. The higher the surface/volume resistivity, the lower the leakage current and the less conductive the material is". [23]

In theory, ideally conducting particles, having infinite conductivities, reach saturation charge instantaneously [4]. However, this is not true for real conductors with finite volume and surface conductivities. It takes particles made of a real conductor, a finite amount of time to attain the maximum amount of charge. This time period can be noted as the actual charging time constant. Surface and volume conductivities, permittivity, contact area with the ground and electric shielding from neighboring particles are all factors that will affect the actual charging time constant and value of the

maximum charge. Theoretical interpretation of the actual charging time constant is sometimes confused with the relaxation time constant that is defined by the material properties. In fact, the previous work [4] has shown that even for a small relaxation time constant, the actual charging time constant can be large due to the high contact resistance between the particles and the ground. Both charging and relaxation time constants can be applied for charging or discharging processes. To differentiate between the two; the actual charging time constant is calculated from the numerical results, dependent on the physical properties of the conducting spherical particle. The relaxation time constant, however, is dependent on material properties of conductivity and permittivity, and is obtained analytically. Little research work has been conducted to study the effect of surface conductivity, electric shielding and proximity effect of other particles on the charging process and the actual charging time constant of particles.

1.2 Objectives

The dynamics of induction charging for spherical particles made of real conductors, with finite volume and surface conductivities and arbitrary permittivities is investigated. The maximum induction charge attained by the spherical particle, and the actual charging time constant are of main interest. Simulations are done in the COMSOL commercial software, which is based on the Finite Element Method. The models were verified by comparing the numerical results with Felici's analytical formulae for regular shaped particles; spheres and hemispheres.

After verifying the simulation models, the particle volume and surface conductivities, and permittivities were varied. The spherical particle's contact area with the ground was also manipulated to vary the contact resistance. The results have shown

that the contact resistance with the ground directly affects the charging time constant of the particle. The main interest, however, was to investigate the effect of surface conductivity on the charging process. The thickness of surface layers was assumed as a small fraction of the particle radius and the results are compared for different cases of surface conductivity.

Since in practical applications, the surface conduction is normally caused by a very thin moisture surface layer, the numeric models were modified to simulate particle charging assuming infinitely thin surface layers. Volume and surface conductivities were chosen to have values reported in practical applications. Agglomerations of spherical particles were also studied using three dimensional transient COMSOL models. The electric shielding and proximity effects were investigated for a pattern of multiple spherical particles. Particles in close proximity with others experience a smaller electric field, and, therefore, accumulate less charge. The arrangement of particles was varied to study the effect of the electric shielding on the spherical particle's saturation charge and actual charging time constant.

Chapter 2
Literature Review

A literature review was conducted on the induction charging of ideally conducting and semi-conducting particles of regular and irregular shapes. Other charging techniques such as corona charging were also reviewed. The research also included particle behaviour in the electric field, the charging time constant and the effect of surface conduction on the charging dynamics. It is shown that extensive research was conducted for charging of regularly shaped particles; however, surface conduction was usually neglected.

2.1 Analytical and experimental work on the induction charging of regularly and irregularly shaped particles

The analytical work was mainly focused on regularly shaped, ideally conducting and semi-conducting particles, as more complicated shapes require numeric tools.

Lebedev and Skal'skaya [3] performed analytical calculations for a conducting sphere. The sphere was resting in a parallel plate capacitor and exposed to a uniform electric field. The sphere's radius was assumed much smaller than the distance between the parallel plates. The results showed that the charge magnitude for a conducting sphere of radius a was $6.56\pi\varepsilon_0 E_0 a^2$.

Félici [2] calculated analytically the magnitude of induction charge on conducting regularly shaped particles. The particles were exposed to a uniform electric field while resting on a grounded plane. He showed that the charge magnitude for a conducting

sphere of radius a was equal to $6.56\pi\varepsilon_0 E_0 a^2$ and $3\pi\varepsilon_0 E_0 a^2$ for a hemisphere. The induction charge was also estimated for an ellipsoid, a semi-ellipsoid and a semi-cylinder.

However, more complicated cases, assuming irregularly shaped particles, require numeric tools; the electric field needs to be calculated first and then the particle's charge can be evaluated. The analytical formulae can be used to validate such numeric models.

Yu [4] presented numerical simulations of induction charging for both regularly shaped conducting particles (sphere, hemisphere and ellipsoid) and irregularly shaped particles modelled by spheres with cosine shaped perturbations on the surface. The simulations were performed using the commercial software COMSOL based on the Finite Element Method. The conducting particle was resting on a grounded electrode and exposed to a uniform electric field. The results showed that a sphere may attain more induction charge than an ellipsoid. For irregularly shaped particles, it was shown that for some level of roughness on the surface of the particle, more charge was accumulated when compared with a smooth sphere. Yu also investigated the dynamics of induction charging of these conducting particles. The surface conduction of the particles was neglected, but different contact areas of the particles with the grounded electrode were studied. The effect of particle contact area, conductivity, and permittivity on the charging dynamics and time constant were investigated. It was shown that an increase in the permittivity and/or conductivity resulted in a faster charging process. Furthermore, increasing the contact area of the particle with the ground decreased the contact resistance, and thereby allowed a faster charging process. The actual charging time constant (calculated from numerical results) was compared with the relaxation time constant for the material. It was shown that there is no direct relation between the

charging time constant and relaxation time constant, but there is a strong effect of the particle's contact resistance on the charging time.

Wu *et al.* [5] investigated the free levitation of particles in an electric field due to the charge induced on the particles by the external field. The electric field strength and particle's size were shown to directly affect the induction charge. The experiment consisted of collecting the levitated particles in a filter contained in a Faraday pail. The Charge to mass ratio (Q/M) was then measured for the samples in the filter. The particle size and shape were measured for spherical and non-spherical particles. For different field strengths, the charge per particle was calculated by combining the results of the charge-to-mass ratio (Q/M), and the particle's surface and volume mean diameters. The results showed that spherical particles (highest volume to surface area ratio) were the hardest to levitate. Non-spherical particles with a surface diameter greater than the volume diameter, accumulated more charge because of a larger surface area. Furthermore, it was shown that increased electric field strength resulted in an increase in the levitated particle size as larger particles require a stronger electric field to levitate. The charge per particle was compared for spherical and non-spherical particles. The results were in good agreement with theoretical prediction. It was shown that the induction charge for the particle was directly affected by the electric field strength and the particle's size, shape and resistivity.

Wu *et al.* [6] further investigated the effect of the electric field strength on the induction charge of free levitating fine particles. The dynamics of the induction charging, charging time, and charge magnitude were shown to be directly affected by the electric field strength and particle size. Wu presented a charging model to show the effect of the

electric field strength and the levitation process of semi-conductive particles. Different models for various particle size and field strengths were tested. The motion of the particles upon levitation was measured by a high-speed digital imaging system. The magnitude of the induction charge of each particle was calculated. The results showed that the charge accumulated by semi-conductive particles was directly affected by the electric field strength: for low electric fields, particles achieved saturation charge prior to liftoff; for higher electric fields, the same particles experienced enough force to levitate before reaching their saturation charge.

Changrag *et al.* [7] also investigated the motion of conductive particles when exposed to a high electrostatic field. They modelled a spherical conductive particle placed in silicone oil to simulate an impurity particle in liquefied plastic. A high-speed camera was used to observe the motion of the sphere. When exposed to a high electrostatic field, the sphere would settle on the lower electrode, then move upward and settle on the upper electrode, before moving back downward. The results showed that the settling time on the electrodes was longer than the predicted charge exchange time; a result of the liquid flow induced by the particle motion. The sphere's velocity decelerated when moving from one electrode to another because of the damping action of the silicone oil layer between the particle and the electrode. The velocity obtained from simulation was different from the theoretical prediction. Furthermore, the results showed that charge accumulated by the sphere could be only half of the estimated theoretical induction charge.

To a less extent, some experimental work was done for different patterns of particle agglomerations. The effect of having an assembly of particles on a given particle's accumulated charge was studied.

Dascalescu *et al.* [8] evaluated the induction charge acquired by cylindrical conductive bodies and the electric force acting on them. Real conductors were simulated as cylinders with various shapes and sizes in contact with a plate electrode and exposed to a non-uniform electric field. Surface charge was evaluated using the Boundary Element Method. The model was extended to form a pattern of conducting and insulating particles. The results showed that the proximity of other bodies reduced the induction charge acquired by the particle, as well as the electric force acting on it.

An alternative method to induction charging is corona charging. However, corona charging involves high voltages, typically in the order of 10-100 kV. On the other hand, induction charging was a preferred method for many industrial applications that involved lower voltages of less than a few kilovolts.

Inculet and Castle [9] constructed a spray unit to inject large volumes of ionic space charge using induction charging. The experimental unit was made of a flat spray sandwiched between two large size induction plane electrodes, which were surrounded by an air curtain to prevent the fine droplets from landing on the electrodes. The charge to mass ratio of the spray droplets were in the order of 4 mC/kg and the ionic charge densities in the order of 2 mC/m^3. The results showed that the large induction electrodes generated excellent induction charging.

2.2 Analytical and experimental work on the effect of surface conduction

The majority of discussed publications related to induction charging of regularly and irregularly shaped particles have neglected surface conduction. However, this effect can be an essential factor in the dynamics of charging of particles. Real conductors with finite conductivities will take a finite amount of time to accumulate maximum charge. This finite time period noted as the actual charging time constant is directly affected by surface conduction. The effect of surface conduction was studied in a few papers related to charge dissipation in liquid tanks and industrial applications.

Adamiak [10] presented a numerical algorithm for simulation of the electric field generated by charged fluid in partially filled cylindrical tanks. The fluid was uniformly charged to a certain level; the charge was then dissipated due to volume and surface conduction. The rate of charge dissipation was calculated by solving in time domain, the current continuity and the electric field equations. The Finite Element Method was used as a numerical tool. The results of simulation show the effect of the surface conduction on the process dynamics: for a high surface conductivity, charge relaxation was much faster. The algorithm presented in [10] could be extended to simulate various conductive bodies and study the effect of volume and surface conduction on the charging and relaxation dynamics.

Pazda *et al.* [11] presented a model of partially filled conducting cylindrical vessels to investigate the relaxation time and the effect of surface conduction. It was shown that for a high surface conductivity the relaxation time for the electric field in the

vapour space was smaller than the charge relaxation time of the liquid; a direct effect of surface conduction on the decay of the electric field.

Pazda *et al.* [12] also presented a general solution for the relaxation of electrostatic charge from an insulating liquid in a columnar vessel of arbitrary cross section. Analytical estimation could be derived for the charge relaxation time of the vessel. Calculation of the electric field distribution and electrostatic potential for the transient model was also possible. Firstly, estimation of the relaxation time was conducted for regularly shaped tanks - in this case cylindrical ones. The model was then extended for irregular geometries. Unknown geometric factors were estimated by reference to known solutions for regular geometries, such as rectangular and cylindrical tanks. The charge relaxation time for the vessel could then be evaluated using all known factors.

Matsubara *et al.* [13] investigated the transient decay of surface potential in an upright cylindrical vessel containing charged liquid with a central fill pipe. Analytical and numerical calculations were done assuming a constant ohmic resistivity. Surface conduction was also assumed, to investigate its effect on the decay of surface charge. The transient problem was solved analytically for the ideal case of the fill pipe extending fully to the vessel bottom. The results showed that for a larger fill pipe, the relaxation rate for the surface potential was modestly faster. For a more practical case when the fill pipe does not reach to the vessel bottom, this problem was studied numerically. The results showed that as long as the fill pipe is submerged in the charged liquid, the relaxation process was negligibly affected. Moreover, charge relaxation was accelerated by higher

surface conduction. However, upon raising the fill pipe above the liquid's surface level, the relaxation rate of the surface potential was dramatically slowed.

Robinson [14] investigated the effect of surface conductivity in industrial applications resulting from electrostatic charges due to particle contamination. Problems included particle contamination from attracting dust, sheets that stick to each other and electrical discharges resulting in damage to electrical components. To overcome these problems, the surface conductivity of the insulating sheets was increased by coating the surface with a conductive layer. Higher surface conduction resulted in faster dissipation of charge. The charge relaxation time was directly dependent on both surface conductivity and geometry. However, charge relaxation was slower, when the distance to the grounded plane decreased, because the tangential electric field needed to drive surface current became smaller.

2.3 Simulation of regularly shaped particles using other charging techniques

Adamiak [15] presented a numerical algorithm to simulate the charging dynamics of high-resistivity spherical particles by the ionic bombardment in an electric field. The algorithm was based on solving the Poisson equation, governing the electric field distribution, and the differential equation expressing the charge conservation law. The Poisson equation was solved by the Finite Element Method, while the conservation equation was solved by the Finite Volume Method. The simulation results showed that saturation charge and charging rate could be predicted for highly conductive particles. However, for high-resistivity particles the solution was more complicated and the

charging time constant was significantly shorter than the relaxation time constant. The technique used to simulate the dynamics of the process could also be extended for the case of induction charging.

Dascalescu *et al.* [16] evaluated the charge acquired by spheres of various dielectric constants placed on the surface of a plate electrode. This was an example for the electro-separation of mixed granular solids. A numerical analysis of the electric field led to the evaluation of the charge acquired by spheres on the surface of the electrode. In addition, experiments were carried out for laboratory set-ups with various types of corona electrodes. An electrometer was used to measure the charge acquired by calibrated spheres of polyamide of 3 mm diameter, when subjected to the positive or negative corona discharge generated between the corona electrode and a metallic rotating roll electrode of 150 mm diameter, connected to the ground. The experimental data were in good agreement with the theoretical predictions; higher applied voltages resulted in an increased corona charging for the particle. However, the results showed that above a threshold voltage of 15kV self discharge of the particle was observed. Furthermore, the charging efficiency was shown to be directly dependent on the type of corona electrode used.

Chapter 3
The Dynamics of Induction Charging of Particles with Finite Volume and Surface Conductivities

3.1 Introduction

3.1.1 Background Theory

In electrostatic fields, the relation between the electric field $\vec{E}$ and electrostatic potential Φ can be described as [1]:

$$\vec{E} = -\nabla\Phi \tag{3-1}$$

In the differential form the electric displacement $\vec{D}$ is governed by Gauss' law as:

$$\nabla \cdot \vec{D} = \rho \tag{3-2}$$

where ρ is the space charge density. Equation (3-2) provides an easy way to calculate the electric fields in symmetric situations.

The absolute permittivity of a material can be described as:

$$\varepsilon = \varepsilon_0 \varepsilon_r \tag{3-3}$$

where ε is the absolute permittivity of the material, ε_0 is the permittivity of vacuum and ε_r is the relative permittivity. In linear and isotropic media, the electric displacement $\vec{D}$ and electric field intensity $\vec{E}$ are parallel:

$$\vec{D} = \varepsilon\vec{E} = \varepsilon_0 \varepsilon_r \vec{E} \tag{3-4}$$

Poisson's equation can be derived from equations (3-1), (3-2) and (3-4) as follows:

$$\nabla^2 \Phi = -\frac{\rho}{\varepsilon} \tag{3-5}$$

For a space charge density of zero, equation (3-5) becomes Laplace's equation:

$$\nabla^2 \Phi = 0 \tag{3-6}$$

At a boundary separating two different media, the tangential component of the electric field (E_{2t} and E_{1t}) and the normal component of the electric displacement (D_{2n} and D_{1n}) must satisfy the continuity equations:

$$E_{2t} = E_{1t} \tag{3-7}$$

$$D_{2n} - D_{1n} = \rho_s \tag{3-8}$$

where ρ_s is the surface charge density at the interface between the two media. The media at both sides of an interface can be conducting, semi-conducting or dielectric. Tangential components of the electric field are shown to be continuous from equation (3-7), whereas a discontinuity is shown in the normal electric displacement component from equation (3-8). Equation (3-8) can be used to calculate the surface charge density and the total charge by:

$$Q_s = \iint \rho_s \, ds = \iint D_{2n} \, ds - \iint D_{1n} \, ds \tag{3-9}$$

Furthermore, Poisson's and Laplace's equations satisfying boundary conditions at the interface between two different media can be used to determine the distribution of the electric field in the entire domain and surface charge density at all interfaces.

3.1.2 Induction charging of a conducting or semi-conducting particle

Induction charging can occur for conducting and semi-conducting materials. In the most typical case, the charged object is grounded and faces a charged electrode, so it is exposed to an electric field. Initially charges move inside the conductor, so that an electric current flows through the material and charges accumulate on the conductor surface. After a certain period of time, the charges will only be present at the conducting surface and the net induced charge inside the material will be zero. Figure 3.1(a) shows a case of a real conductor, represented by a spherical particle, with a surface conducting layer. This representation forms the basis of the simulations done in this thesis. When the particle is exposed to an electric field directed downwards, positive charges are induced on the lower part of the sphere and negative charges on the upper part. The positive charges on the lower part of the sphere attract negative charges from the ground electrode, creating a current from this electrode into the particle. Since the negative charges on the upper part of the sphere can move freely, the particle acquires more negative charge. After a certain period of time, negative charges accumulate on the surface of the particle as shown in Figure 3.1(b), with a magnitude and distribution that produces zero field and thus zero net induced charge inside the conductor.

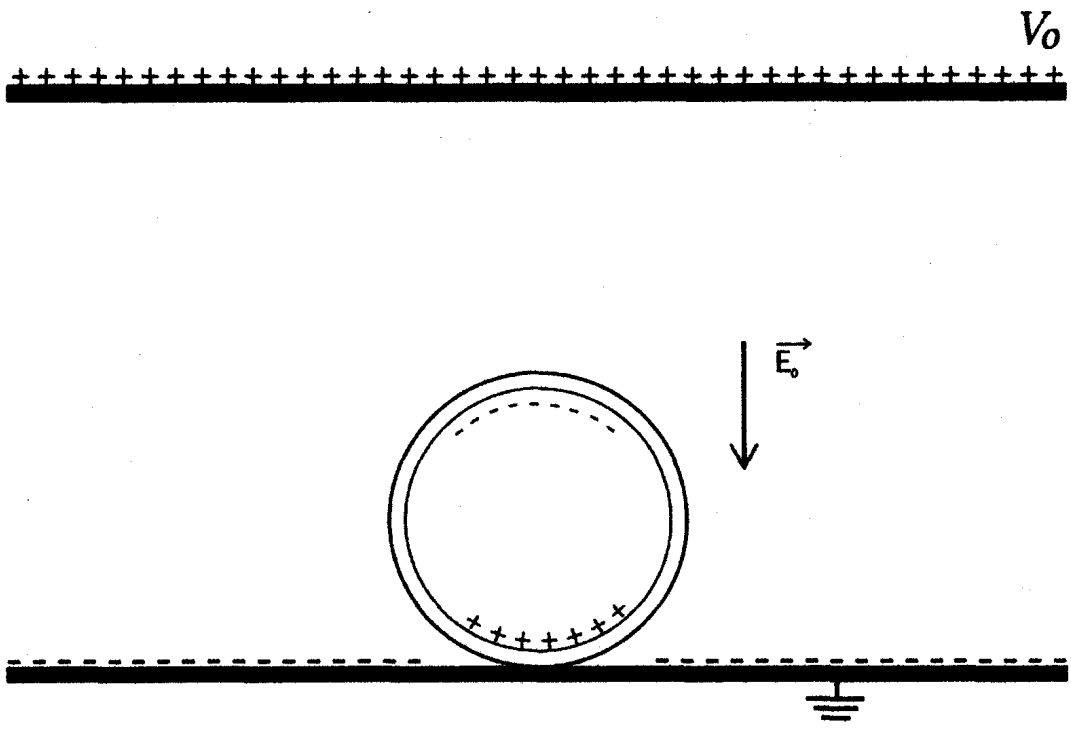

Figure 3.1(a) Induction charging of a conducting particle – polarization charge.

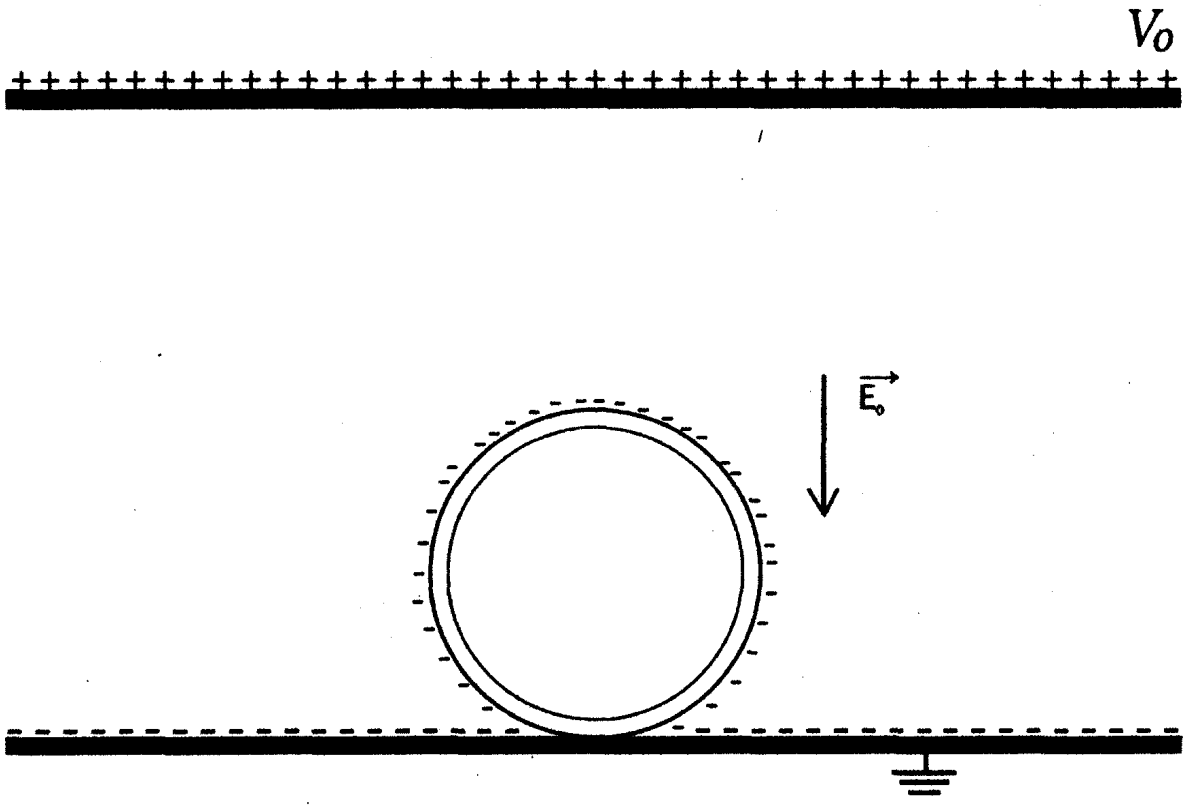

Figure 3.1(b) Induction charging of a conducting particle – net induced charge.

The relationship between the current density $\vec{j}$ and the surface charge density ρ_s is given as:

$$\vec{j} = \sigma \vec{E} \tag{3-10}$$

$$\rho_s = \int_0^t J_n \, dt \tag{3-11}$$

where J_n is the normal component of the current density, σ is the volume conductivity of the particle and $\vec{E}$ is the electric field present inside the particle.

In some electrostatic applications, surface conduction is important as it directly affects the charging dynamics of a given material. For the induction charging of a real conductor, represented by a spherical particle, both volume and surface conductivities are defined. In general, for a volume with a surface layer, surface conductivity can be defined using the equation of a resistance as:

$$R = \frac{l}{\sigma a d} = \frac{l}{\sigma_s a} \tag{3-12}$$

where R is the resistance of the material, l is the length of the layer, a the width of the layer, d the thickness of the layer, σ volume conductivity of the material and σ_s surface conductivity of the surface layer as shown in Figure 3.2.

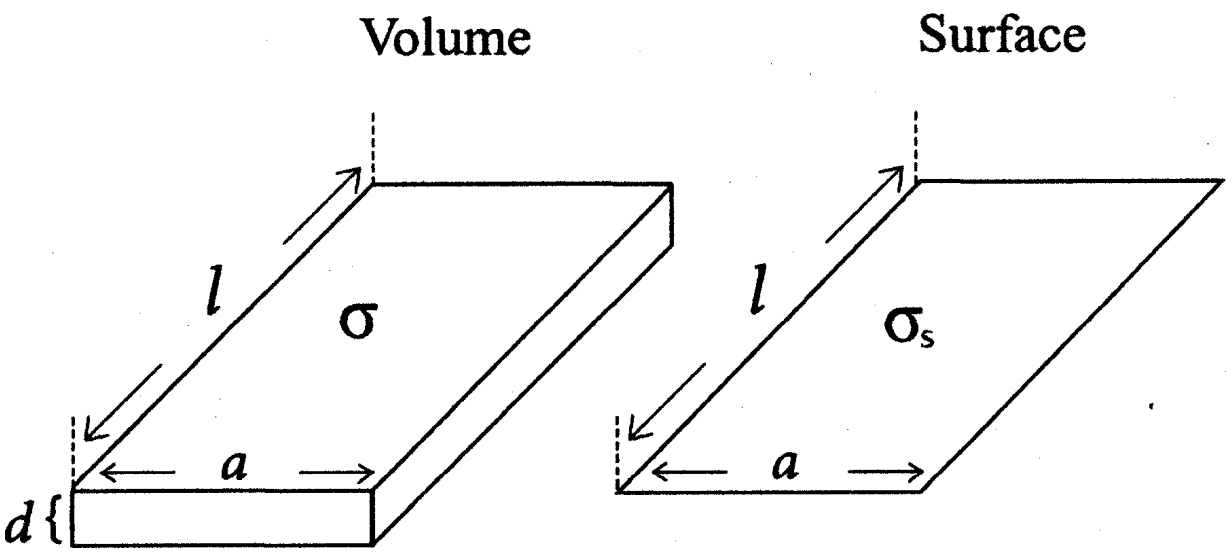

Figure 3.2 Volume and surface conductivities for the material and surface layer.

Based on equation (3-12) the equation for surface conductivity is seen to be:

$$\sigma_s = \sigma d \tag{3-13}$$

Surface conductivity is calculated per square of the surface layer. Surface conductance can then be calculated by multiplying surface conductivity by total number of squares in the surface layer.

The charging process of the particle can be described in terms of the time it takes for the charge to reach its saturation value. This is directly affected by the volume and surface conductivities. The charge as a function of time can be expressed as:

$$Q(t) = Q_s(1 - e^{-t/\tau_c}) \tag{3-14}$$

where Q_s is the saturation charge of the material and τ_c the actual charging time constant. For $t = \tau_c$ equation (3-14) reduces to:

$$Q(\tau_c) = Q_s(1 - 1/e) = 0.632Q_s \tag{3-15}$$

Therefore, the actual charging time constant can be defined as the time after which the particle would accumulate 63.2% of its saturation charge. Saturation time t_{sa} is also sometimes defined as:

$$t_{sa} = 5\tau_c \tag{3-16}$$

The particle can be considered to have reached saturation when it accumulates 99.3% of its predicted saturation charge. The charging time constant τ_c can also be described analytically in terms of resistance R and capacitance C as [17]:

$$\tau_c = RC \tag{3-17}$$

Equation (3-17) is often used in circuit models to define the charging time constant across an RC circuit. The discharging time constant τ_d is also equal to RC. For a discharging process of the particle, the loss of charge can be described as:

$$Q(t) = Q_0 e^{-t/\tau_d} \tag{3-18}$$

where τ_d is the actual discharge time constant. The discharge time constant is sometimes confused with the relaxation time constant which is a property of the bulk material that depends upon the conductor permittivity and conductivity parameters as:

$$\tau_r = \varepsilon/\sigma \tag{3-19}$$

where τ_r is the relaxation time constant, ε the particle permittivity and σ the particle's volume conductivity.

For a conducting spherical particle in contact with a grounded electrode, it was noticed by Yu [4] that the actual charging time constant τ_c is directly affected by the geometry and the contact resistance of the particle with the grounded electrode. The relaxation time constant τ_r however, was shown to be independent of the particle's geometry or contact resistance (3-19); depending only on the material's permittivity and conductivity. Therefore, there is no direct relation between the relaxation time constant and the actual charging time constant for this situation.

3.2 Mathematical and Equivalent Circuit Models

3.2.1 Mathematical Model

The model analyzed in this chapter is a spherical particle with a surface conducting layer as shown in Figure 3.3.

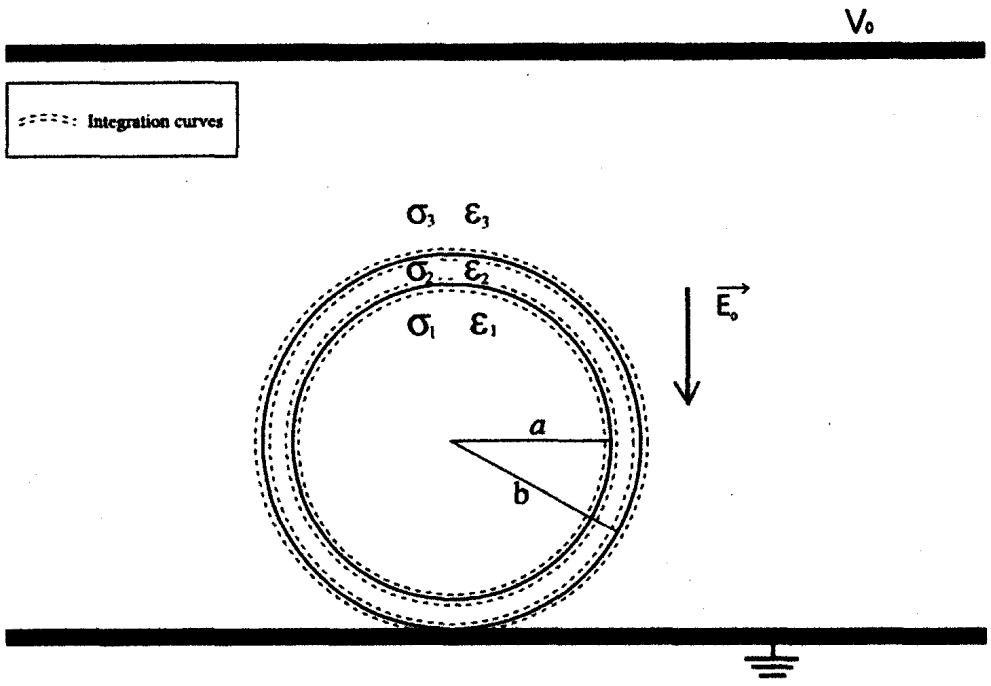

Figure 3.3 Conducting spherical particle with a finite conducting surface layer resting on a grounded electrode and exposed to an external electric field.

The inner sphere represents the bulk particle with a radius a = 1.5mm and the outer sphere (radius b) represents the surface layer of the particle with varying thicknesses. Initially, the radius of the outer sphere was b = 1.65mm, corresponding to 10% of the particle radius. This radius was reduced in further simulations to study the effect of surface conductivity. The integration curves, shown surrounding the outer and inner spheres, were used for calculation of surface charge density at each interface. For the inner sphere (Region 1), the finite volume conductivity and permittivity were defined as σ_1 and ε_1, respectively. For the outer sphere, i.e. the surface layer of the particle (Region 2), these parameters were defined as σ_2 and ε_2, respectively. For the air region (Region 3), the parameters were assigned as σ_3 and ε_3, respectively. However, for the air region σ_3 is zero as the ambient gas is non-conductive, and $\varepsilon_3 = \varepsilon_0 = 8.854 \times 10^{-12}$ F/m. Figure 3.4 shows the three media described in this model.

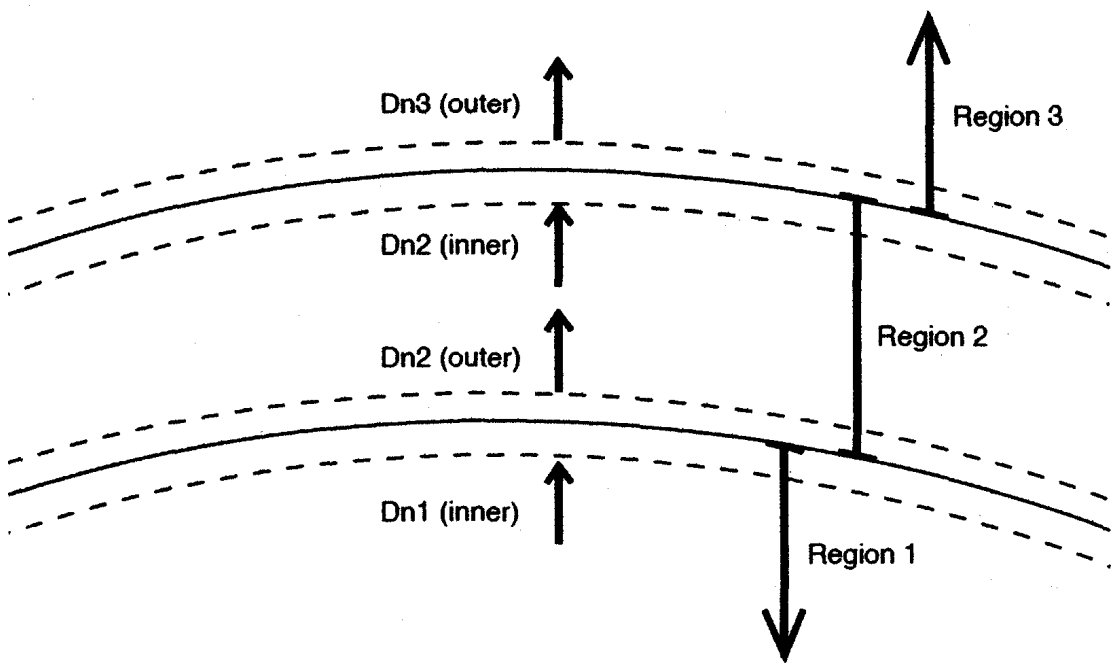

Figure 3.4 Definition of regions and integration surfaces for spherical particle with conducting surface layer.

The spherical particle was in contact with a grounded electrode and faced a positively charged electrode at a distance of 0.1m, as shown in Figure 3.3. The voltage applied to the charged electrode was 50 kV and, therefore, created a downward electric field of 0.5MV/m. Both spheres representing the particle and surface layer had finite volume conductivities and permittivities. The electric potential distribution is governed by Laplace's equation (3-6).

From equation (3-8) the boundary conditions can now be described for the three media as:

$$D_{n3(\text{outer})} - D_{n2(\text{inner})} = \rho_{s2} \tag{3-20}$$

$$D_{n2(\text{outer})} - D_{n1(\text{inner})} = \rho_{s1} \tag{3-21}$$

where ρ_{s2} is the surface charge density on the outer sphere and ρ_{s1} is the surface charge density on the inner sphere. Consequently, the saturation charge at each surface can be calculated by:

$$Q_{s2} = \iint \rho_{s2}\, ds_2 \tag{3-22}$$

$$Q_{s1} = \iint \rho_{s1}\, ds_1 \tag{3-23}$$

3.2.2 Equivalent circuit for the conducting spherical particle

The equivalent circuit model for the conducting spherical particle is discussed to investigate the relations between the actual charging time constant and the material relaxation time constant. To simplify analysis, the equivalent circuit for a conducting spherical particle without a surface layer is shown in Figures 3.5 (a) and (b).

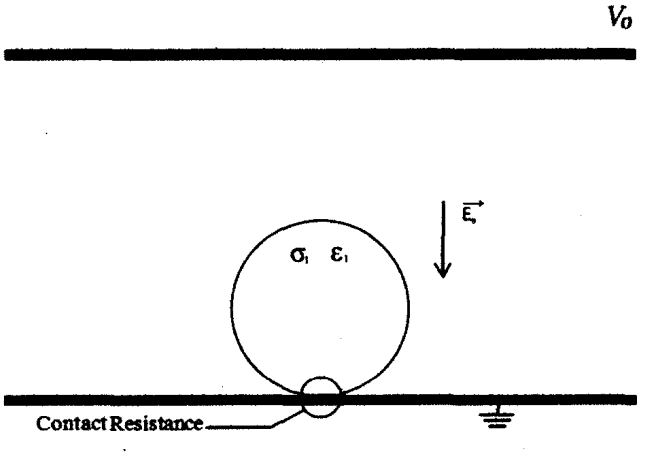

Figure 3.5 (a) Conducting spherical particle without a surface layer

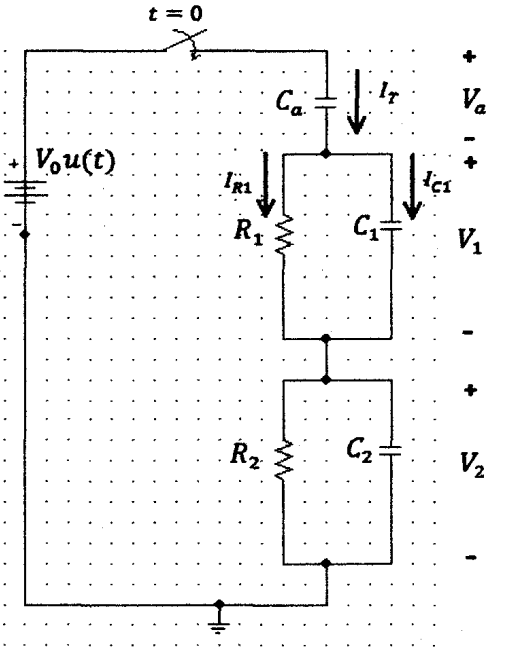

Figure 3.5 (b) Equivalent circuit for conducting spherical particle without a surface layer

The capacitance C_a represents the air gap between the particle and the upper electrode. The R_1C_1 circuit represents the spherical particle with actual material properties: real conductivity and permittivity. Time constant $\tau_1 = R_1C_1$ is analogous to the relaxation time constant τ_r and depends on material properties.

The R_2C_2 circuit represents the contact area between spherical particle and the grounded electrode. Time constant $\tau_2 = R_2C_2$ depends on the contact area and particle conductivity.

At time $t = 0$, the upper electrode as shown in Figure 3.5(a) is charged. In the equivalent circuit, the source voltage is connected to capacitor C_a, and circuits R_1C_1 and R_2C_2 as shown in Figure 3.5(b). The source voltage $V(t)$ can be expressed in terms of a unit step function $u(t)$ as:

$$V(t) = V_0 u(t) \tag{3-24}$$

The currents $I_T(t)$, $I_{C1}(t)$ and $I_{C2}(t)$ across C_a, C_1 and C_2 respectively can be expressed as:

$$I_T(t) = \frac{C_a dV_a(t)}{dt} \tag{3-25}$$

$$I_{C1}(t) = \frac{C_1 dV_1(t)}{dt} \tag{3-26}$$

$$I_{C2}(t) = \frac{C_2 dV_2(t)}{dt} \tag{3-27}$$

where $V_a(t)$, $V_1(t)$ and $V_2(t)$ are the voltages across capacitors C_a, C_1 and C_2 respectively, and are functions of $V(t)$. From equation (3-24) it is shown that the source voltage has a step function, and therefore the derivative of this step function results in an impulse function $\delta(t)$, showing a discontinuity in the currents across the capacitors from $t = 0^-$ to $t = 0^+$.

The voltage $V_1(t)$ in terms of $I_T(t)$ for the parallel R_1C_1 circuit can be expressed as [17]:

$$V_1(t) = (V_1(0) - I_T(t)R_1)\, e^{-t/R_1C_1} + I_T(t)R_1 \tag{3-28}$$

where $V_1(0)$ is the initial voltage across C_1. Similarly, the voltage $V_2(t)$ is given by:

$$V_2(t) = (V_2(0) - I_T(t)R_2)\, e^{-t/R_2C_2} + I_T(t)R_2 \tag{3-29}$$

where $V_2(0)$ is the initial voltage across C_2. The impulse function of $I_T(t)$ would explain the discontinuity of the capacitor voltages $V_1(t)$ and $V_2(t)$ from $t = 0^-$ to $t = 0^+$. When compared to the particle charging model, this agrees with the theoretical prediction; as soon as the upper electrode is charged, a voltage appears between the upper surface of the particle and the ground plate.

Charge accumulation for the particle is compared for different instances of time, to verify the circuit results with the theoretical predictions for the particle charging model. Firstly, the voltages from equations (3-28) and (3-29) are not sufficient for calculation at time $t = 0^+$ because the voltage would be the unknown initial condition. Therefore, the capacitor voltages $V_a(t)$, $V_1(t)$ and $V_2(t)$ are calculated assuming the

capacitive voltage divider method. To simplify analysis, the voltage drop between the upper part of the particle and the grounded electrode is expressed as $V_{12}(t)$ where $V_{12}(t) = V_1(t) + V_2(t)$ in the circuit. Consequently, the charge between the upper part of the particle and the grounded electrode is $Q_{12}(t)$ and the equivalent capacitance for C_1 and C_2 is C_{12}. The charge in the air gap between the upper part of the particle and the upper electrode is expressed as $Q_a(t)$ having a voltage drop $V_a(t)$. Assuming a capacitive voltage divider, $V_a(t)$ and $V_{12}(t)$ can be calculated at $t = 0^+$:

$$V_a(0^+) = \frac{C_{12}}{C_a + C_{12}} V_0 \tag{3-30}$$

$$V_{12}(0^+) = \frac{C_a}{C_a + C_{12}} V_0 \tag{3-31}$$

Consequently $Q_a(t)$ and $Q_{12}(t)$ can be calculated at $t = 0^+$:

$$Q_a(0^+) = \frac{C_a C_{12}}{C_a + C_{12}} V_0 \tag{3-32}$$

$$Q_{12}(0^+) = \frac{C_a C_{12}}{C_a + C_{12}} V_0 \tag{3-33}$$

The charge $Q_p(t)$ accumulated on the particle is given by:

$$Q_p(t) = Q_a(t) - Q_{12}(t) \tag{3-34}$$

It was shown from equations (3-32) and (3-33) that $Q_a(0^+) = Q_{12}(0^+)$. Therefore $Q_p(0^+) = 0$ from equation (3-34). For the particle model, at $t = 0^+$, charge has not

accumulated on the surface of the particle yet which is in excellent agreement with the analytical result ($Q_p(0^+) = 0$).

The current $I_T(\infty)$ is zero (current across capacitor at steady state). Therefore, $V_{12}(\infty) = 0$, and $Q_{12}(\infty) = 0$ which indicates that there is no charge inside the conductor. Substituting in equation (3-34), $Q_p(\infty) = Q_a(\infty)$; which means all the charge is accumulated on the particle surface at steady state. The behaviour of the circuit agrees with theoretical predictions of the charge build up for the spherical particle model.

From this equivalent circuit, two time constants can be identified. To a first approximation the actual charging time constant (τ_c) will be a function of τ_1 and τ_2. Assuming $\tau_c = \tau_1 + \tau_2$ because R_1C_1 and R_2C_2 are in series:

τ_1 is primarily dependent on the material properties, analogous to τ_r;

τ_2 is primarily dependent on the contact resistance and particle geometry;

- If $\tau_2 = 0$ that is zero contact resistance (infinitely large contact area); $\tau_c \rightarrow \tau_1$.
- If $\tau_2 \gg \tau_1$ that is having a large contact resistance (very small contact area); $\tau_c \rightarrow \tau_2$.
- If τ_1 and τ_2 are of the same order; assumption that $\tau_c = \tau_1 + \tau_2$.

Therefore, only for the case where zero contact resistance exists, the actual charging time constant will approach the material relaxation time constant, which are often misinterpreted to be the same. These conclusions also agree with the research work conducted by Yu [4]. Even for a small material relaxation time constant, the actual

charging time constant can be large due to high contact resistance between the particle and the ground (small contact area).

For the spherical particle with a surface layer, the model and equivalent circuit can be represented as shown in Figures 3.6 (a), (b) and (c).

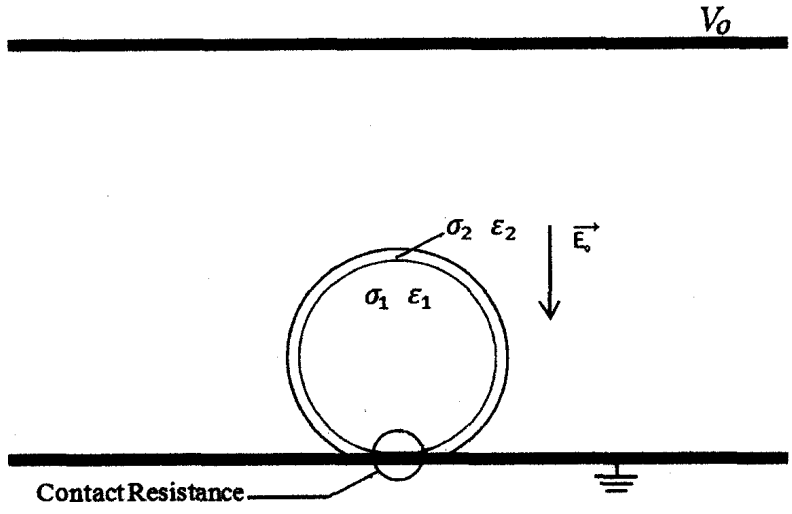

Figure 3.6(a) Conducting spherical particle with surface layer.

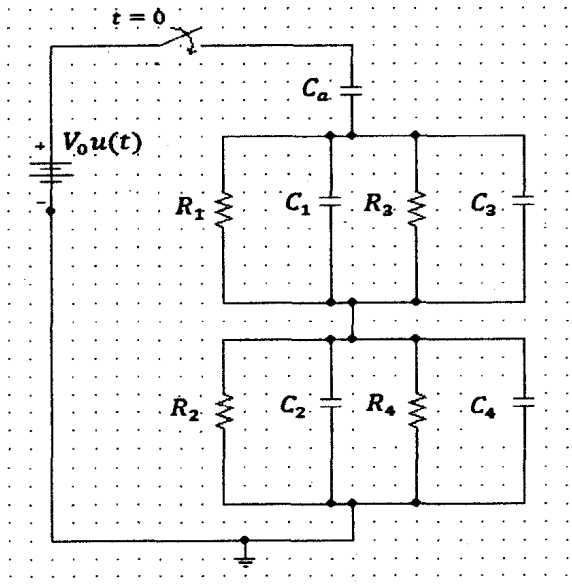

Figure 3.6(b) Equivalent circuit for conducting spherical particle with surface layer.

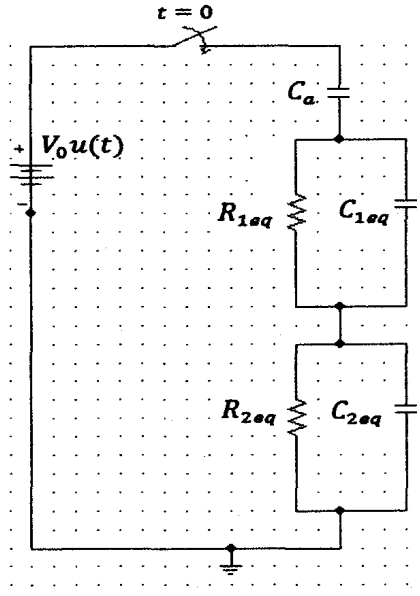

Figure 3.6(c) Simplified equivalent circuit.

The circuit parameters are:

C_a : The air gap between the particle and the upper electrode.

R_1C_1: The particle with actual material properties: real conductivity and permittivity.

R_3C_3: The surface layer of the particle with conductivity and permittivity

R_2C_2: The contact area between the particle and the grounded electrode.

R_4C_4: The contact area between the surface layer and the grounded electrode.

$R_{1eq}C_{1eq}$: The equivalent circuit of R_1C_1 // R_3C_3.

$R_{2eq}C_{2eq}$: The equivalent circuit of R_2C_2 // R_4C_4.

The RC circuits representing the surface layer and its contact area with the ground are assumed to be in parallel with the bulk particle and its contact area with the ground. This is because the path of the current entering the contact point would be either through the bulk material or through the surface layer.

When compared to previous analysis for the particle without a surface layer, the nature of the circuit and the analysis for the time constants do not change upon adding a surface layer; only the values of the RC circuits would be affected. In this case, time constant $\tau_1 = R_{1eq}C_{1eq}$ depends on material properties of the bulk particle and its surface layer. $\tau_2 = R_{2eq}C_{2eq}$ depends on contact areas of the bulk particle and surface layer with the grounded electrode.

3.3 Simulation Model

The model was investigated using the COMSOL commercial software Version 3.2 [20]. This software is based on the Finite Element Method and is a convenient numerical tool to solve partial differential equations over a continuous and finite domain. The Finite Element Method [19] requires that the entire domain is discretized into some number of small elements. These elements are defined by nodes and the set of equations is formulated for all nodal values of an unknown solution.

The geometry of this model is fairly simple. The two electrodes are represented with a rectangle of width 0.5m and height 0.1m. The lower electrode was grounded, while the upper electrode was supplied with 50 kV. For the transient case, the voltage supplied was represented as V = 50,000 * (t > 0). The vertical sides of the rectangle were set as electric insulators.

Initially, two concentric spheres are drawn with respective radii of 1.65mm and 1.5mm (radii values are varied in later simulations as the outer radius is reduced to achieve a reduced layer thickness). Figure 3.7 illustrates the representation of the model. Two-dimensional models with axial symmetry were created in COMSOL. Therefore, it was sufficient to model the two concentric spheres as semi-spheres with symmetry axis on the z-axis. The outer sphere represents the surface layer with finite thickness (d) and the inner sphere represents the particle itself. The spherical particle had varying contact areas with the grounded electrode. For most cases, a finite small contact area of 0.039mm^2 with the ground was specified, and compared with a point contact and several

larger contact areas. The volume conductivities, permittivities, and surface layer thickness were also varied to compare the results for different cases.

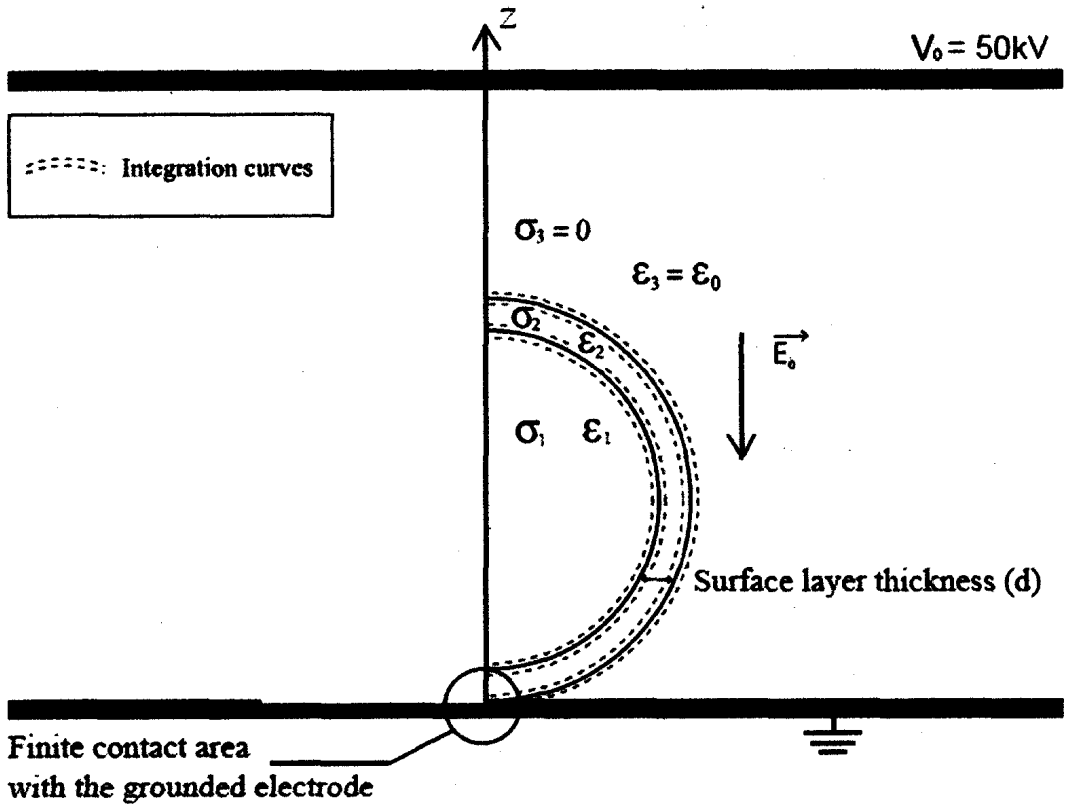

Figure 3.7 Geometric model of the conducting spherical particle in COMSOL

To integrate the surface charge density and calculate the charge magnitude, artificial surfaces (integration curves) were drawn surrounding the outer and inner spheres as shown in Figure 3.7. The artificial curves have radii of length ±0.02mm from the actual curves. This is done to evaluate the normal component of the electric displacement vectors, to get the surface charge density as described by equations (3-20) and (3-21) and shown in Figure 3.4. Direct integration of these equations can be done on COMSOL using equations (3-22) and (3-23) to calculate the charge magnitude.

Finally, upon modelling the geometry of the problem and defining all parameters, the whole domain was meshed. Fine triangular discretizations were produced in the surface conducting layer, which is required for accurate results. The mesh pattern was refined for many trials and the simulation results were tested for accuracy. The refined pattern shown in Figure 3.8 achieved accurate results and was chosen for the simulations, as further refining of this pattern resulted in less than 0.001% error.

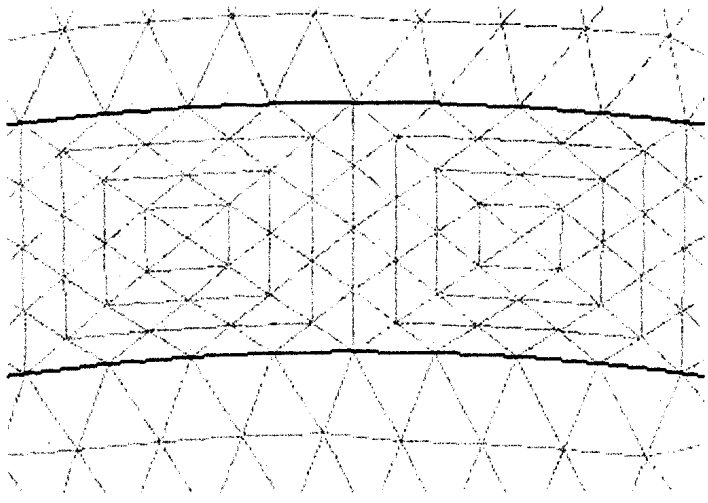

Figure 3.8 Fine discretization in the surface layer of the particle

The simulations were conducted in the transient mode to study the dynamics of the charging process. The total charge accumulated by the particle, surface charge densities on the outer and inner spheres, and the charging time constant were calculated.

3.4 Model Verification

The first step in this process was to validate the simulation model by comparing the value of saturation charge of the spherical particle calculated by COMSOL, with the analytical results calculated from Felici's formula [2]. For this purpose, a verification of

the induction charge for both a sphere having a point contact with the grounded electrode and a hemisphere was performed, and the results are shown in Table 3.1. The initial values used for particle radius, volume conductivity and permittivity were similar to parameters chosen by Yu [4]. This allowed further verification and comparison to previous work performed on simulation of spherical particles without a surface layer.

Table 3.1 Comparison between the saturation charge from analytical and numerical solutions

Particle Shape	Felici's Formulae [2]	Induction Charge $\|Q\|$(pC) (Felici)	Induction Charge $\|Q\|$(pC) (COMSOL)	Percentage Difference (%)
Hemisphere (a=1.5mm, b=1.65m)	$3\pi\varepsilon_0 E_0 b^2$	113.5922	113.5921	-0.0001%
Sphere (a=1.5mm, b=1.65m)	$6.56\pi\varepsilon_0 E_0 b^2$	248.388	249.1	0.29%

The results show a very small error between the analytical and numerical values for both shapes. This small error range, 0.0001 for a hemisphere and 0.3% for a sphere, was identical to previous work performed by Yu [4]. In this situation, the 10% outer layer thickness was assumed identical to the interior by setting the outer and inner conductivities to be equal ($\sigma_1 = \sigma_2$ = 1nS/m) and the relative permittivity ε_r= 3.

. Figures 3.9 and 3.10 show the induction charge build up for both shapes, to verify the resultant saturation charge as described in Table 3.1 earlier. The rate of the charge build up will be discussed in detail in further simulations.

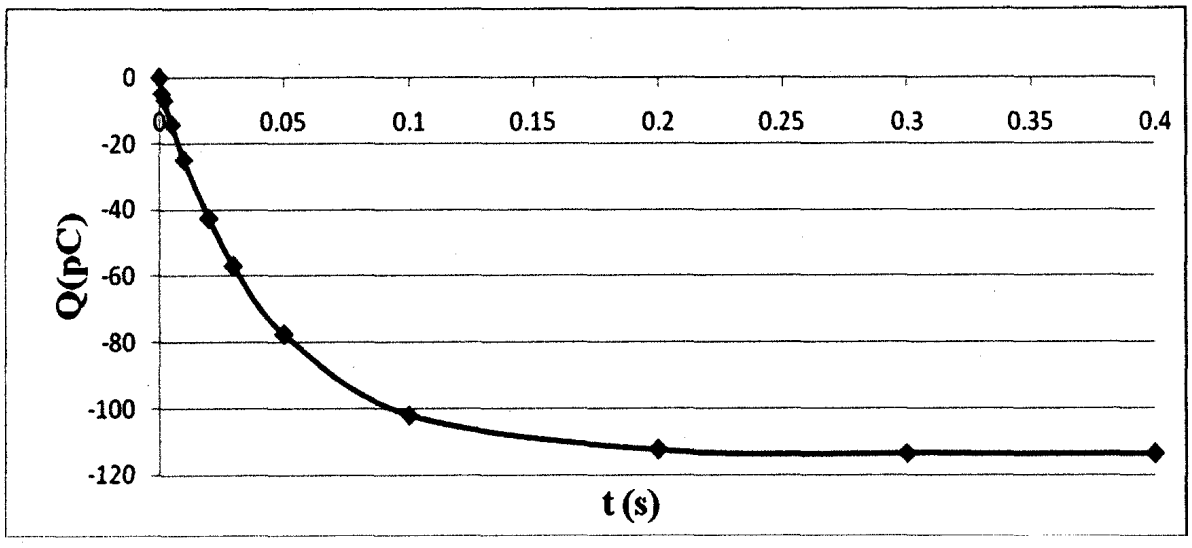

Figure 3.9 Induction charge Q versus time t for the hemisphere with 10% surface layer thickness assuming $\sigma_1 = \sigma_2 = 1$nS/m and $\varepsilon_r = 3$.

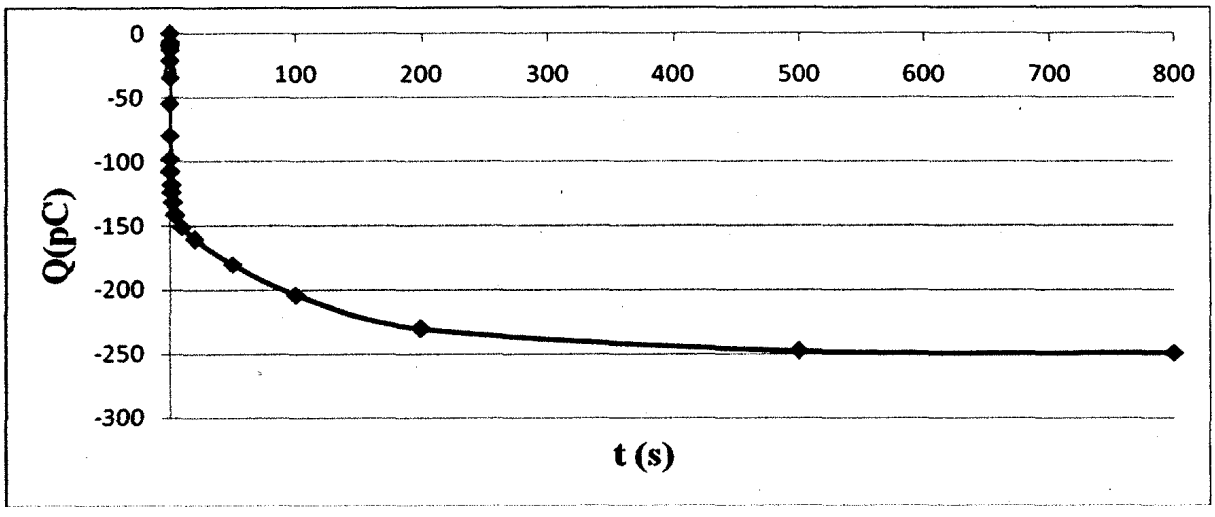

Figure 3.10 Induction charge Q versus time t for the sphere with 10% surface layer thickness assuming $\sigma_1 = \sigma_2 = 1$nS/m and $\varepsilon_r = 3$ (a point contact with grounded electrode).

3.5 Spherical particle with a 4.27% surface layer thickness

Having the simulation model verified, the surface layer thickness was decreased to 4.27% of the particle radius, as this was the lowest thickness that can be achieved with

the geometric limitations of the COMSOL software. As a result, the particle had an inner radius a = 1.5mm and an outer radius b = 1.564mm.

3.5.1 Spherical particles with different contact areas

The simulations were conducted for a spherical particle having a surface layer thickness of 4.27% of the particle radius with a constant relative permittivity ε_r= 3 in both layers. Two cases were compared with different conductivities of the particle and its surface layer. In the first case, the outer conductivity was chosen to be greater than the inner conductivity ($\sigma_2 > \sigma_1$) with σ_2 = 1nS/m and σ_1 = 0.1nS/m. For the second case, the outer conductivity was chosen to be less than the inner conductivity ($\sigma_2 < \sigma_1$) with σ_2 = 0.1nS/m and σ_1 = 1nS/m. Five different contact areas were assumed: a point contact, 0.039mm^2, 0.13mm^2, 0.61mm^2 and 7.68mm^2 (hemisphere). The contact area between the particle and the ground creates a finite resistance that slows the charging process. An ideal point contact would create infinite resistance and the particle would never be charged. However, in numerical models, a point contact will be represented as a small, but unknown, finite contact area due to discretization of the domain. For this reason, a small finite contact area is usually preferred over a point contact in numerical models.

The simulation results for the different contact areas were compared, assuming different conductivities. The plots for the induction charge Q on the outer surface of the particle as a function of time t for the different contact areas are shown in Figures 3.11 and 3.12. The hemisphere plot is excluded from the graph because of a scaling issue and is represented in the tables that follow.

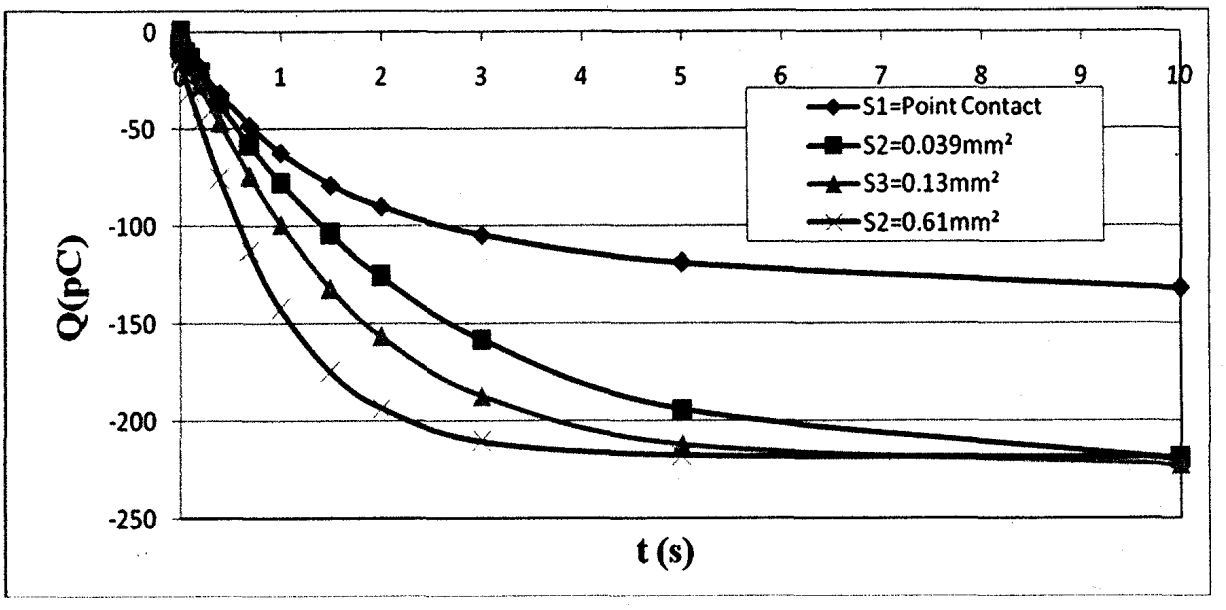

Figure 3.11 The induction charge Q on the outer surface versus time t for the particle with 4.27% surface layer thickness assuming σ_2 = 1nS/m and σ_1 = 0.1nS/m ($\sigma_2 > \sigma_1$) for different contact areas between the particle and the ground.

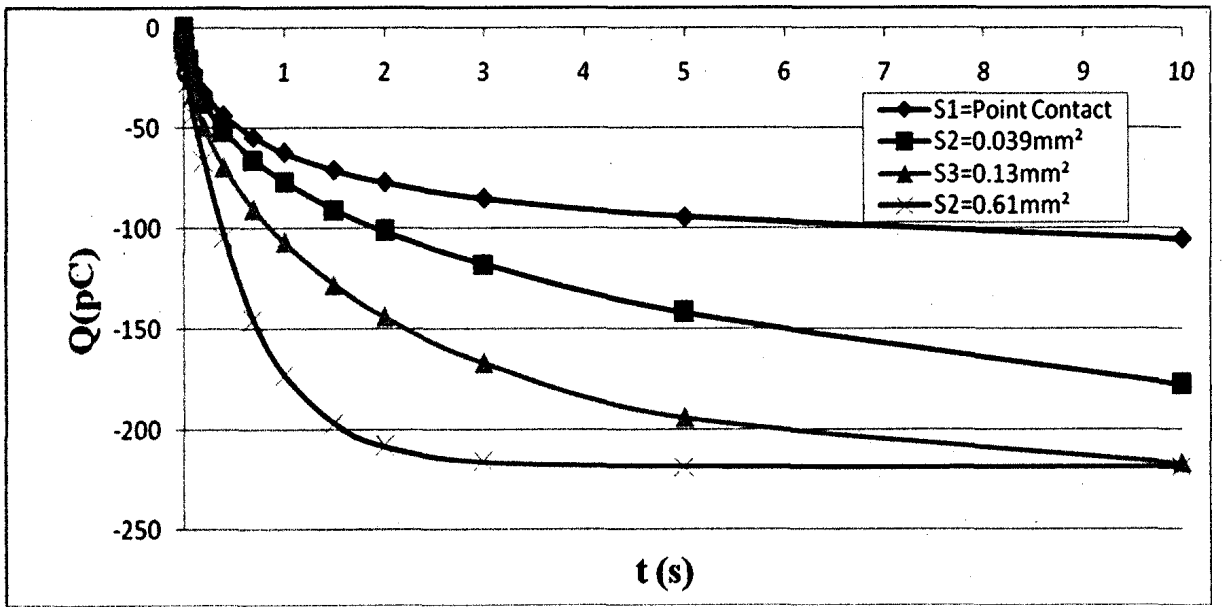

Figure 3.12 The induction charge Q on the outer surface versus time t for the particle with 4.27% surface layer thickness assuming σ_2 = 0.1nS/m and σ_1 = 1nS/m ($\sigma_2 < \sigma_1$) for different contact areas between the particle and the ground.

Table 3.2 Charging dynamics for the particles with different contact areas assuming $\sigma_2 > \sigma_1$

Contact Area	Saturation Charge Q_s(pC)	Actual Charging Time Constant τ_c(s)	Relaxation Time Constant τ_r(s) ($\tau_r = \varepsilon_1/\sigma_1$)	τ_c/τ_r
S1=0 (Point Contact)	-223.84	19.5	0.266	73.31
S2=0.039mm²	-223.52	2.42	0.266	9.10
S3=0.13mm²	-222.71	1.6	0.266	6.02
S4=0.61mm²	-218.67	0.9	0.266	3.38
S5=7.68mm² (Hemisphere)	-102.06	0.07	0.266	0.26

Table 3.3 Charging dynamics for the particles with different contact areas assuming $\sigma_2 < \sigma_1$

Contact Area	Saturation Charge Q_s(pC)	Actual Charging Time Constant τ_c(s)	Relaxation Time Constant τ_r(s) ($\tau_r = \varepsilon_1/\sigma_1$)	τ_c/τ_r
S1=0 (Point Contact)	-223.84	175	0.0266	6578.95
S2=0.039mm²	-223.52	4.9	0.0266	184.21
S3=0.13mm²	-222.71	1.9	0.0266	71.43
S4=0.61mm²	-218.67	0.65	0.0266	24.44
S5=7.68mm² (Hemisphere)	-102.06	0.09	0.0266	3.38

From Tables 3.2 and 3.3 it can be seen that the sphere with a point contact takes the longest time to reach saturation, as the actual charging time constant is the highest when compared to the particles with finite contact areas. The material relaxation time constant is calculated analytically for the bulk particle. In all cases where the contact area increases, the actual charging time constant τ_c and the ratio of the actual charging time constant to the material relaxation time constant (τ_c/τ_r) decrease. This is also shown in Figures 3.11 and 3.12 as the charge accumulation is fastest for particles having the largest contact areas. The results show that a smaller contact area results in an increased resistance at the contact with the ground, which slows the charging process.

For the case of a point contact, τ_c was shown to be much greater than τ_r ($\tau_c \gg \tau_r$). This is due to the high resistance between the particle and the grounded electrode. The saturation charge for the particle with a point contact was shown to be -223.84pC which agrees with the result obtained by Felici's formula for the spherical particle (-223.17pC) with a 0.3% error difference. The hemisphere has the fastest charging time with a saturation charge of -102.06pC which also agrees with the analytical formula by Felici for the hemisphere (-102.59pC) with an error difference of 0.009%.

The results of the actual charging time constants when compared with the material relaxation time constant agree with the time constants' predictions from the equivalent circuitry model discussed in an earlier section. For a particle with point contact (very high contact resistance), the actual charging time constant is affected mainly by the contact area rather than material properties. For a hemi-sphere (large contact area i.e.

small contact resistance) the actual charging time constant is affected mainly by the material properties in this case the real conductivity of the particle.

Tables 3.2 and 3.3 also show that $|Q_s|$ decreases from a value of 223.84pC to 102.06pC as the contact area increases. This is because the surface area of the sphere is decreasing as the contact area increases. For all cases where $\sigma_2 > \sigma_1$, the actual charging times are faster than those for $\sigma_2 < \sigma_1$, assuming the same contact areas. An outer conductivity that is greater than an inner conductivity ($\sigma_2 > \sigma_1$), results in a larger current flow and, therefore, faster accumulation of charge. From all the cases studied, the actual charging time constant is shown to be geometry related as it is dependent on the contact area with the ground, and particle's inner and outer conductivities.

3.5.2 Conductivity effect of the particle and its surface layer

Firstly, a small finite contact area was chosen for the spherical particle because an ideal point contact does not exist in practical applications. Moreover, a point contact in numerical models actually means a very small, but undefined, contact area. The results presented in the previous section also showed that a particle having a point contact with the grounded plate was charged very slowly, when compared to particles with finite contact areas. For this reason, simulations were performed on particles with a known and small finite contact area with the grounded plate; in this case a 0.039mm^2 contact area was chosen.

Charge accumulation on the outer surface of the particle

Two cases are considered, the first model having $\sigma_2 > \sigma_1$ where σ_2 = 1nS/m and σ_1 = 0.1nS/m; the second model having $\sigma_2 < \sigma_1$, where σ_2 = 0.1nS/m and σ_1 = 1nS/m. Both cases have an identical relative permittivity of ε_r = 3. Figure 3.13 shows the results of the simulation for the charge build up on the outer surface of the spherical particle.

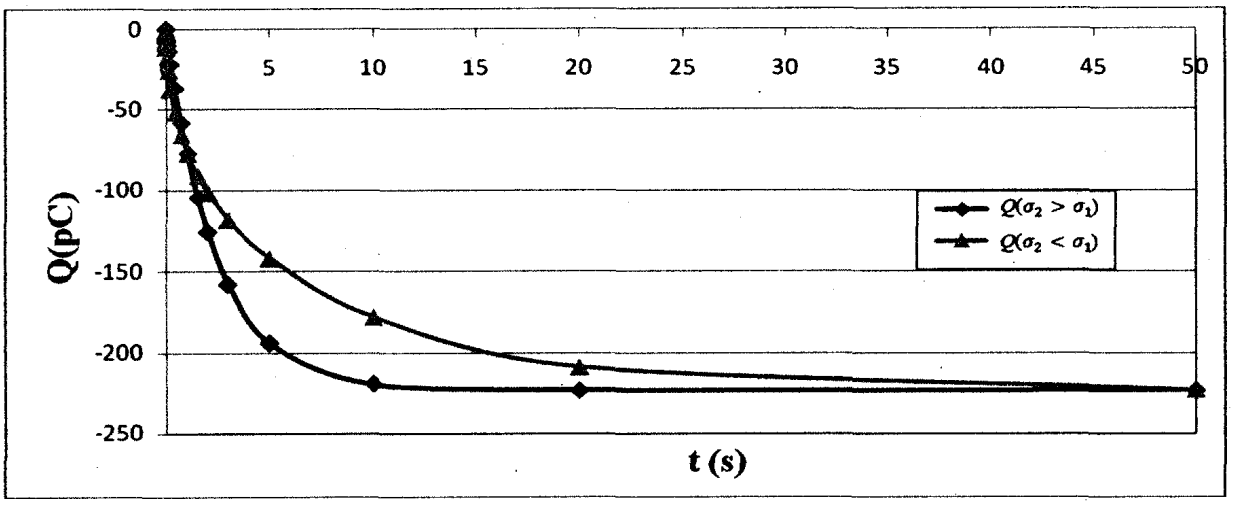

Figure 3.13 Induction charge Q on the outer surface versus time t for the particle with 4.27% surface layer thickness assuming different conductivities and ε_r = 3 (0.039mm² contact area with the ground).

The results are summarized in Table 3.4, which shows the effect of varying conductivity of the conducting surface layer and the inner sphere (σ_2 and σ_1).

Table 3.4 Charging dynamics for particles with different conductivities

Sphere with 0.039mm² contact area	Saturation Charge Q_s(pC)	Actual Charging Time Constant τ_c(s)	Relaxation Time Constant τ_r(s) ($\tau_r = \varepsilon_1/\sigma_1$)	τ_c/τ_r
$\sigma_2 > \sigma_1$ (σ_2=1nS/m, σ_1=0.1nS/m)	-223.52	2.42	0.266	9.10
$\sigma_2 < \sigma_1$ (σ_2=0.1nS/m, σ_1=1nS/m)	-223.52	4.9	0.0266	184.21

From Table 3.4 it can be seen that the actual charging time for the particle with a more conductive outer surface ($\sigma_2 > \sigma_1$) is faster than that of the particle with a less conductive outer surface ($\sigma_2 < \sigma_1$). This can also be seen in Figure 3.13 as the particle having $\sigma_2 > \sigma_1$ reaches saturation much faster than the particle with $\sigma_2 < \sigma_1$. In both cases, the particle reaches the same saturation value. For comparison purposes the conductivity values have been held consistent with those described earlier, and the relative permittivity value was set to 3.0 in both cases.

For a fixed finite contact area in both simulations, it is shown that the actual charging time constant is affected by the conductivities of the bulk particle and its surface layer. Therefore as shown in the previous section, the actual charging time for the particle is not only geometry related (dependent on contact area) but also material related (dependent on inner and outer conductivities in this case). For example, the ratio τ_c/τ_r increases from 9.10 to 184.21 when changing from a high surface conductive layer to a less surface conductive one.

Charge accumulation on surface of the inner sphere

The same model was used to calculate the charge accumulation on the outer surface of Region 1, which is the surface of the inner sphere as shown in the adjacent figure. Again two cases were considered, the first model having $\sigma_2 > \sigma_1$, where σ_2 = 1nS/m and σ_1 = 0.1nS/m; the second model having $\sigma_2 < \sigma_1$, where σ_2 = 0.1nS/m and σ_1 = 1nS/m. Both cases have a fixed relative permittivity of ε_r = 3. Figures 3.14 and 3.15

show the results of the simulation for the charge build up on the inner surface of the sphere.

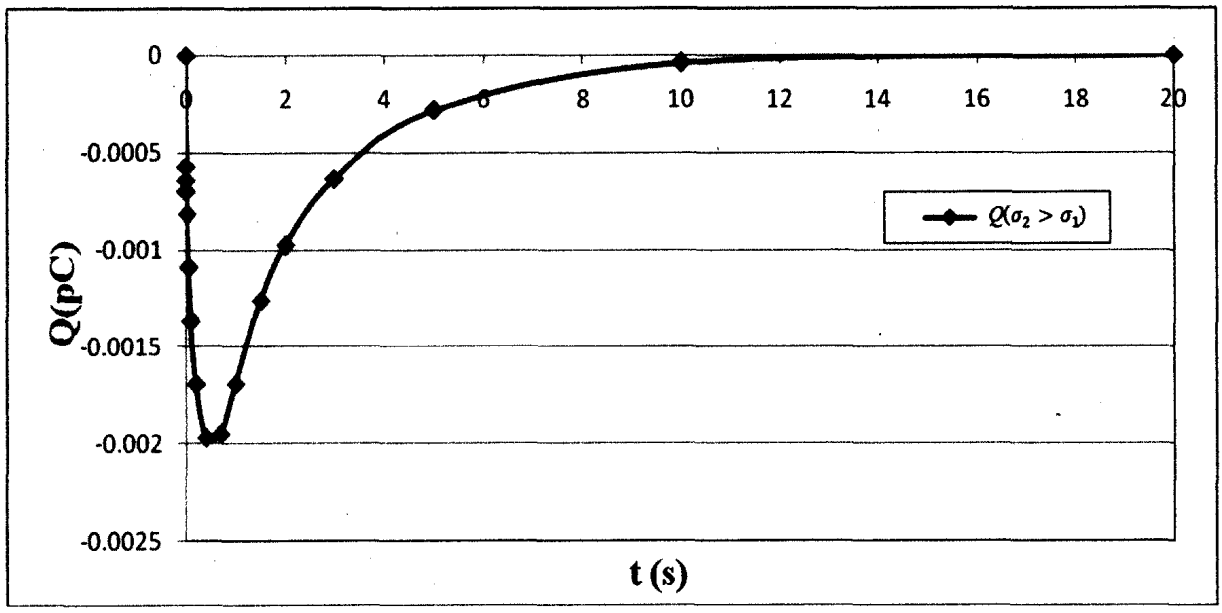

Figure 3.14 Charge Q on the outer surface of Region 1 versus time t for the particle with 4.27% surface layer thickness assuming σ_2 = 1nS/m, σ_1 = 0.1nS/m and ε_r = 3 (0.039mm² contact area with the ground).

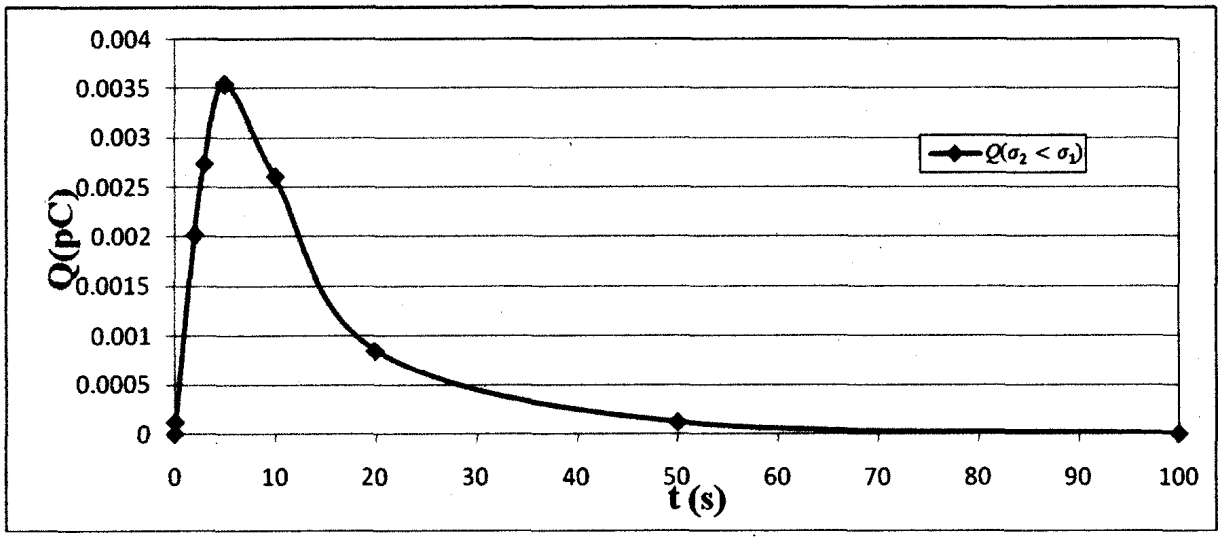

Figure 3.15 Charge Q on outer surface of Region 1 versus time t for the particle with 4.27% surface layer thickness assuming σ_2 = 0.1nS/m, σ_1 = 1nS/m and ε_r = 3 (0.039mm² contact area with the ground).

From Figures 3.14 and 3.15 it can be seen that at first, some charge builds up on the outer surface of Region 1, and then it disappears. This can be explained as follows: at first an electric field exists inside the particle, resulting in the charge accumulation on the outer surface of Region 1. The charge would continue to move until a net zero electric field is produced within the particle. When this stage is reached, the charge accumulated on the inner surface between the particle and the surface layer dissipates. The difference in the polarity of the accumulated charge can be seen from Figures 3.14 and 3.15, and can be further explained referring to Figures 3.16 (a) and (b) explaining the case where $\sigma_2 < \sigma_1$.

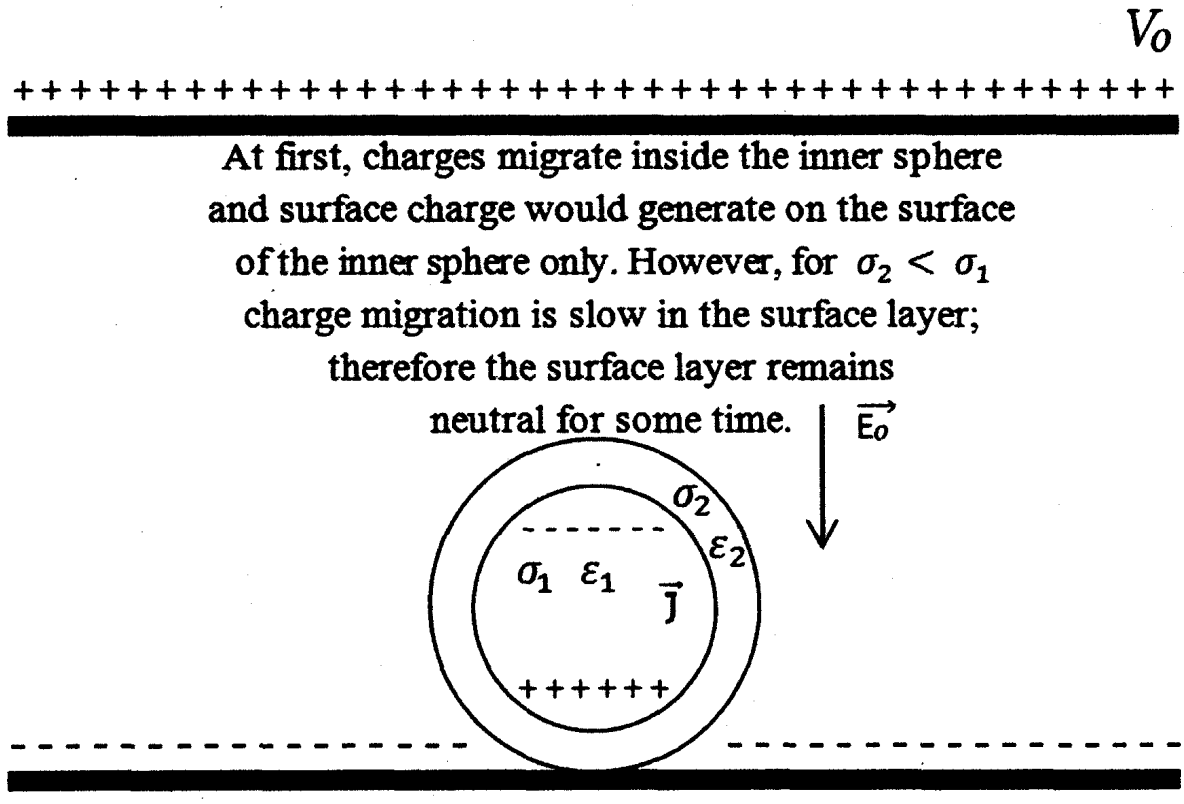

Figure 3.16 (a) Particle with a conducting surface layer exposed to an external electric field assuming $\sigma_2 < \sigma_1$ (Initial state upon exposure to electric field).

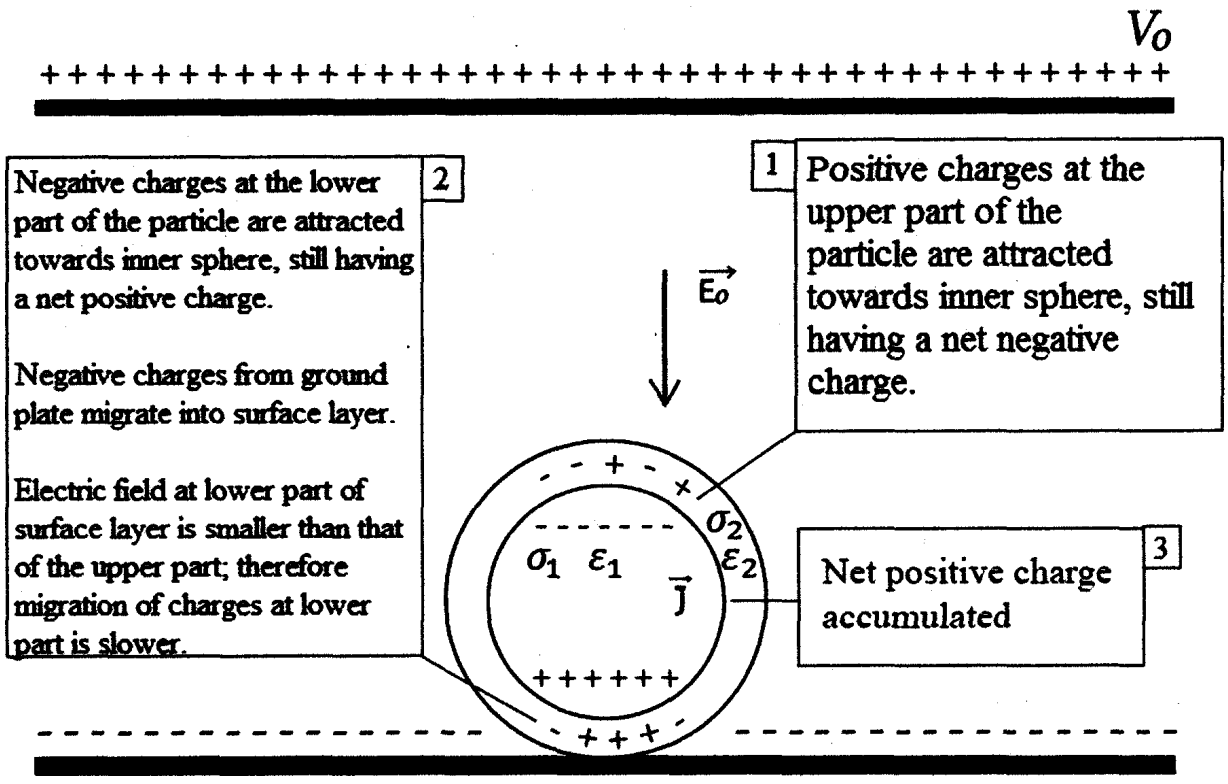

Figure 3.16 (b) Particle with a conducting surface layer exposed to an external electric field assuming $\sigma_2 < \sigma_1$ (Charge migration after some time).

A positive voltage is applied on the upper electrode, whereas the lower electrode is grounded. At first the negative charges are attracted to the upper inner sphere, and positive charges to the lower inner sphere as shown in Figure 3.16 (a). For $\sigma_2 < \sigma_1$, as shown in Figure 3.16 (b) the inner sphere is more conductive than the surface layer, and charge migration to the surface layer would be slow. The electric field at the lower part of the surface layer is smaller than that of the upper part due to negative charges from the ground plate; therefore migration of charges at lower part is slower. The net effect is the following: decay of the original positive charge on the lower part of the inner sphere is slower than decay of the negative charge on the upper part of the sphere; therefore net positive charge is present at the surface of the inner sphere.

When the particle reaches steady state the electric field inside is zero and, therefore, a net induced charge would only be distributed on the outer surface of Region 2 (surface layer of particle) and there is no charge on the inner sphere.

As for the case where $\sigma_2 > \sigma_1$, shown in Figure 3.14, the negative charges would flow at first on the surface layer due to the high conductivity of this surface. The result is a net negative charge on the inner surface.

An illustration to show the effect of having a larger contact area of 0.13mm² is shown in Figure 3.17.

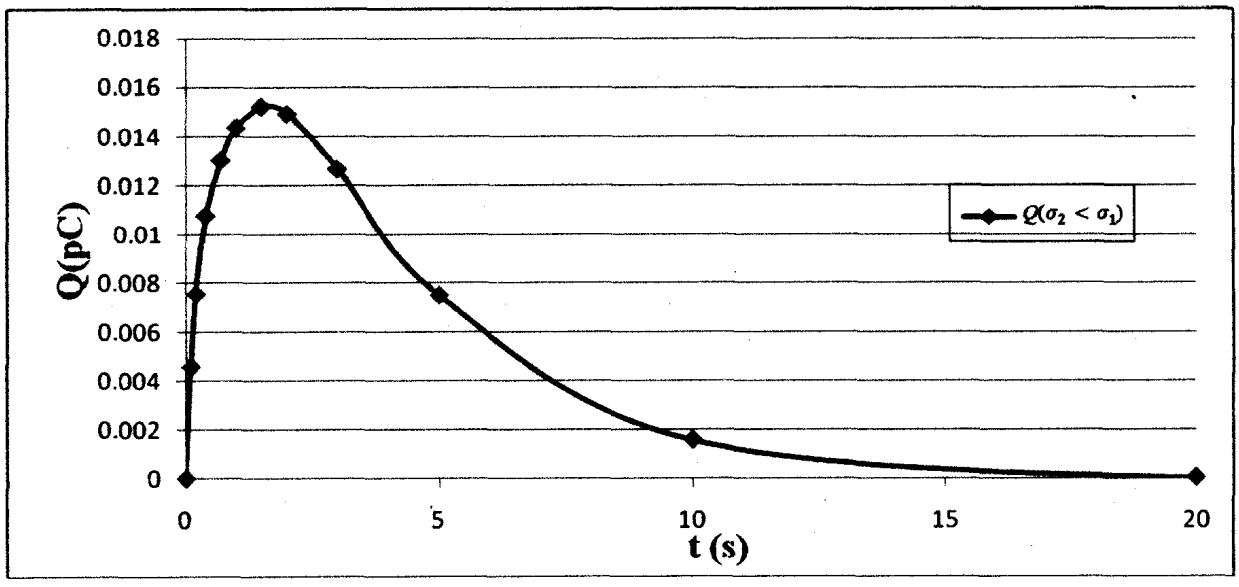

Figure 3.17 Charge Q on the inner surface versus time t for the particle with 4.27% surface layer thickness assuming $\sigma_2 = 0.1$nS/m, $\sigma_1 = 1$nS/m and $\varepsilon_r = 3$ (0.13mm² contact area with the ground).

When comparing Figure 3.17 (0.13mm² contact area with grounded electrode) to Figure 3.15 (0.039mm² contact area with grounded electrode), it can be seen that the charge build up and decay on the surface of the inner sphere is faster for larger contact

areas. For the larger contact area, resistance into the lower part of the sphere is smaller and, therefore, the negative charges are easily attracted to the lower inner sphere. As a conclusion, the contact area has been shown to affect directly the contact resistance between the spherical particle and ground plate, and therefore the charge on the inner surface.

3.5.3 The effect of particle permittivity

To investigate the effect of the particle permittivity on the charging dynamics, the particle with a 4.27% surface layer was used. Two cases were simulated: the first case having $\sigma_2 > \sigma_1$ where σ_2 = 1nS/m and σ_1 = 0.1nS/m; the second case having $\sigma_2 < \sigma_1$ where σ_2 = 0.1nS/m and σ_1 = 1nS/m. The contact area of the particle with the grounded electrode was 0.039mm^2. For the surface layer of the particle (Region 2), the relative permittivity ε_{r2} was set to 3 in all cases. For the inner sphere representing the bulk particle (Region 1), the relative permittivity ε_{r1} was set to 3 and 10 to study cases of increasing the particle's permittivity. Figures 3.18 and 3.19 show the simulation results for $\sigma_2 > \sigma_1$ and $\sigma_2 < \sigma_1$ respectively with different permittivities.

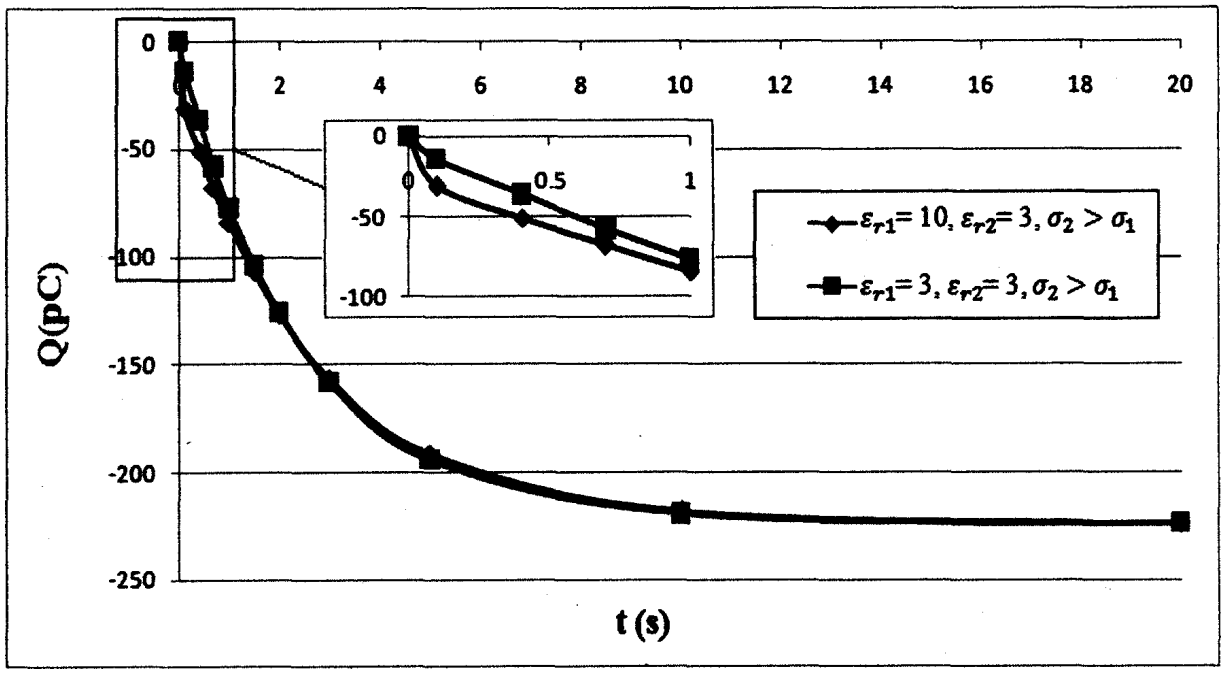

Figure 3.18 Induction charge Q on the outer surface versus time t for the particle with 4.27% surface layer thickness assuming $\sigma_2 > \sigma_1$ and different permittivities (0.039mm² contact area with ground).

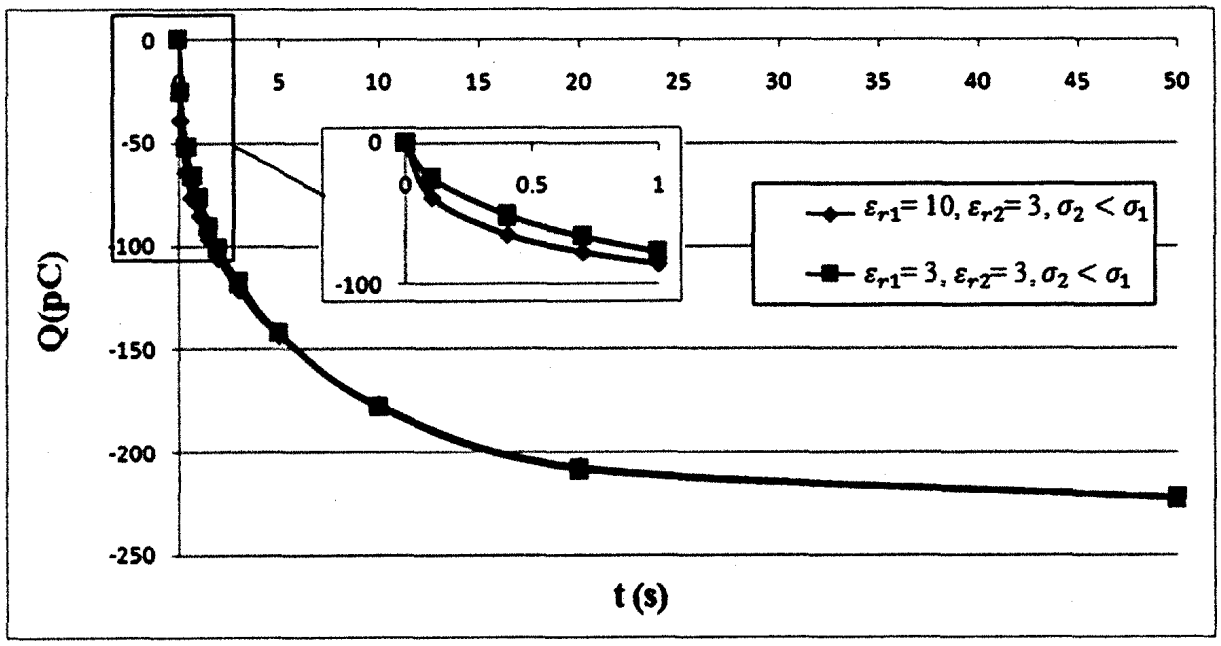

Figure 3.19 Induction charge Q on the outer surface versus time t for the particle with 4.27% surface layer thickness assuming $\sigma_2 < \sigma_1$ and different permittivities (0.039mm² contact area with ground).

Table 3.5 Charging dynamics for particles with different conductivities and permittivities

Relative Permittivity (ε_{r1})	Conductivity σ (nS/m)	Saturation Charge Q_s(pC)	Actual Charging Time Constant τ_c(s)	Relaxation Time Constant τ_r(s) ($\tau_r = \varepsilon_1/\sigma_1$)	τ_c/τ_r
3	$\sigma_2 > \sigma_1$ (σ_2=1, σ_1=0.1)	-223.52	2.42	0.266	9.10
10	$\sigma_2 > \sigma_1$ (σ_2=1, σ_1=0.1)	-223.52	2.38	0.885	2.69
3	$\sigma_2 < \sigma_1$ (σ_2=0.1, σ_1=1)	-223.52	4.9	0.0266	184.2
10	$\sigma_2 < \sigma_1$ (σ_2=0.1, σ_1=1)	-223.52	4.6	0.0885	51.98

From Table 3.5 it can be seen that in all cases the particle reaches the same saturation charge, however, at slightly different charging rates. For the first case, where $\sigma_2 > \sigma_1$ the particle having a relative permittivity (ε_{r1} = 10) accumulates charge slightly faster than a particle having (ε_{r1} = 3). As shown in Figures 3.18 and 3.19, except for the initial stage, the curves almost coincide, resulting in a very small difference in the actual charging time constant when varying the inner permittivity from 3 to 10. This is also the case when the inner conductivity is set to be larger than the outer conductivity. The actual charging time constant shows a slightly bigger difference, but still the two graphs appear to almost coincide.

The ratio τ_c/τ_r decreases with the increase of the relative permittivity. As the results show, the permittivity seems to be less effective than the conductivity of the particle and its surface layer. Referring to Table 3.5 for identical permittivities, decreasing the conductivity by a factor of 10 shows that the actual charging time constant increases from 2.42 seconds to 4.9 seconds and from 2.38 seconds to 4.6 seconds. However, decreasing the relative permittivity from 10 to 3 for identical conductivities shows that the actual charging time constant increases slightly from 2.38 seconds to 2.42 seconds and from 4.6 seconds to 4.9 seconds. Therefore, the actual charging time constant is more affected by conductivity of the spherical particle than by its permittivity, and is not directly proportional to the particle's permittivity.

3.6 Spherical particle with a 1% surface layer thickness

Further decreasing the surface layer thickness with separate calculation of the charge accumulation on the outer and inner surfaces of the particle (Region 2 and Region 1, respectively) was not possible due to geometric limitations on COMSOL. However, when considering only the total charge on the spherical particle, the geometrical model was simpler and modeling a further decrease in the surface layer thickness was possible. The model simulated is a spherical particle with a finite contact area of 0.039mm^2 and a 1% surface layer thickness. The plots for the total charge Q as a function of time t for different combinations σ_2 and σ_1 are shown in Figure 3.20. In the first case it was assumed that $\sigma_2 > \sigma_1$ where σ_2 = 1nS/m and σ_1 = 0.1nS/m; in the second case it was

assumed that $\sigma_2 < \sigma_1$ where σ2 = 0.1nS/m and σ1 = 1nS/m. The relative permittivity for both simulations was kept constant at 3.

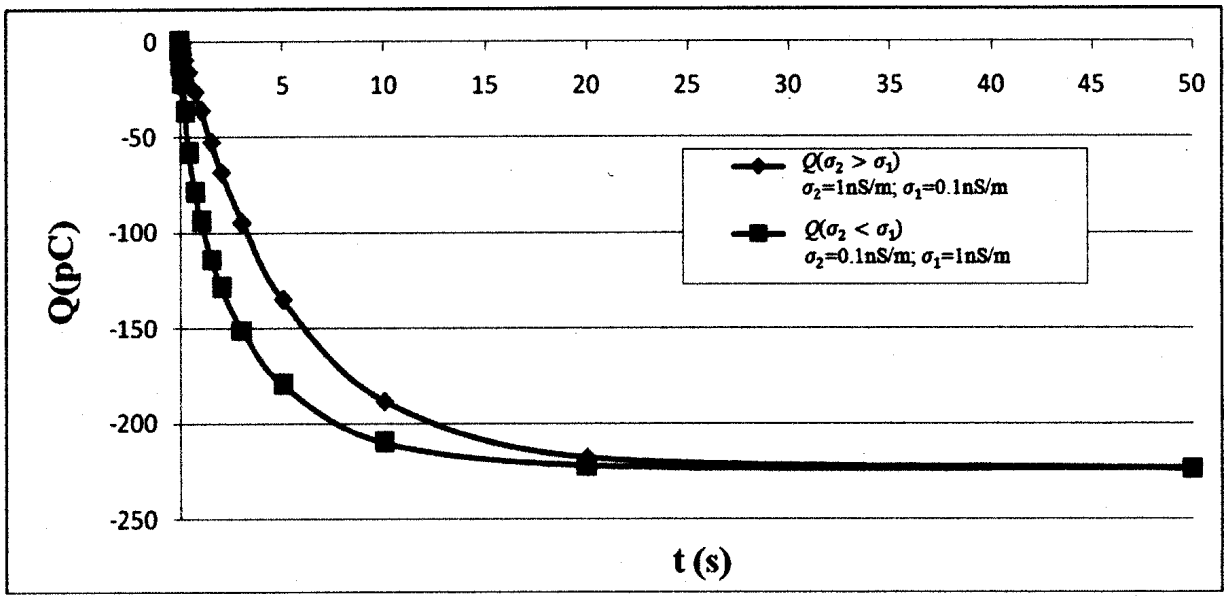

Figure 3.20 The total charge Q versus time t for the particle of 1% surface layer thickness with a 0.039mm² contact area with the ground, relative permittivity = 3 and varying conductivities.

Table 3.6 Charging dynamics for particle with different conductivities, relative permittivity = 3 and 1% surface layer thickness

Sphere with 0.039mm² contact area and 1% layer thickness	**Saturation Charge Q_s(pC)**	**Actual Charging Time Constant τ_c(s)**	**Relaxation Time Constant τ_r(s) ($\tau_r = \varepsilon_1/\sigma_1$)**	τ_c/τ_r
$\sigma_2 > \sigma_1$ (σ_2=1nS/m, σ_1=0.1nS/m)	-223.52	5.84	0.266	21.95
$\sigma_2 < \sigma_1$ (σ_2=0.1nS/m, σ_1=1nS/m)	-223.52	2.4	0.0266	90.23

From Table 3.6 it can be seen that unlike the previous cases, where the spherical particle accumulates charge faster with a more conductive surface layer, the sphere with a thin 1% surface layer behaves in the opposite fashion: the charging process is slower for $\sigma_2 > \sigma_1$. This shows the effect of the surface layer thickness on the actual charging time constant, as a more conductive inner sphere ($\sigma_2 < \sigma_1$) will accumulate charge faster than a sphere with a more conductive outer surface ($\sigma_2 > \sigma_1$). This is because, the effective surface area is much thinner when using a 1% thickness, and the inner conductivity (σ_1) is the main factor affecting the contact resistance and thus the actual charging time constant.

From Figure 3.20 it can be seen that the charge accumulation is faster for the case where $\sigma_2 < \sigma_1$. The results from Table 3.6 show the actual charging time constant increases from 2.4 seconds to 5.84 seconds when decreasing σ_1 by a factor of 10. The ratio τ_c/τ_r increases when increasing σ_1 because the material relaxation time constant of the bulk particle drops from 0.266 to 0.0266 seconds. As a conclusion, the actual charging time constant is not only directly affected by the sphere's contact area with the ground, and the conductivity values, but also significantly depends on the surface layer thickness.

3.6.1 The effect of surface layer thickness

In the previous section, the significant effect of the surface layer thickness on the charge accumulation has been shown. Further results in this section are provided to investigate the effect of different surface layer thicknesses on the dynamics of charge

accumulation by the spherical particle. The model used has a contact area of 0.039mm² with the ground, and a constant relative permittivity of 3. Table 3.7 and Figure 3.21 show the actual charging time constants for different surface layer thicknesses when compared to different conductivity ratios of 0.01, 0.1, 0.5, 2, 10, and 100 respectively. σ_2 is fixed at 1nS/m and σ_1 is varied to achieve the mentioned ratios.

Table 3.7 The actual charging time constant versus conductivity ratios for different surface layer thicknesses

σ_2/σ_1	0.01	0.1	0.5	2	10	100
τ_c(s) 10% Layer	0.67	0.73	0.87	1.16	1.58	1.82
τ_c(s) 4.27% Layer	0.41	0.49	0.75	1.38	2.42	3.2
τ_c(s) 1% Layer	0.142	0.25	0.71	2.12	5.84	11.62

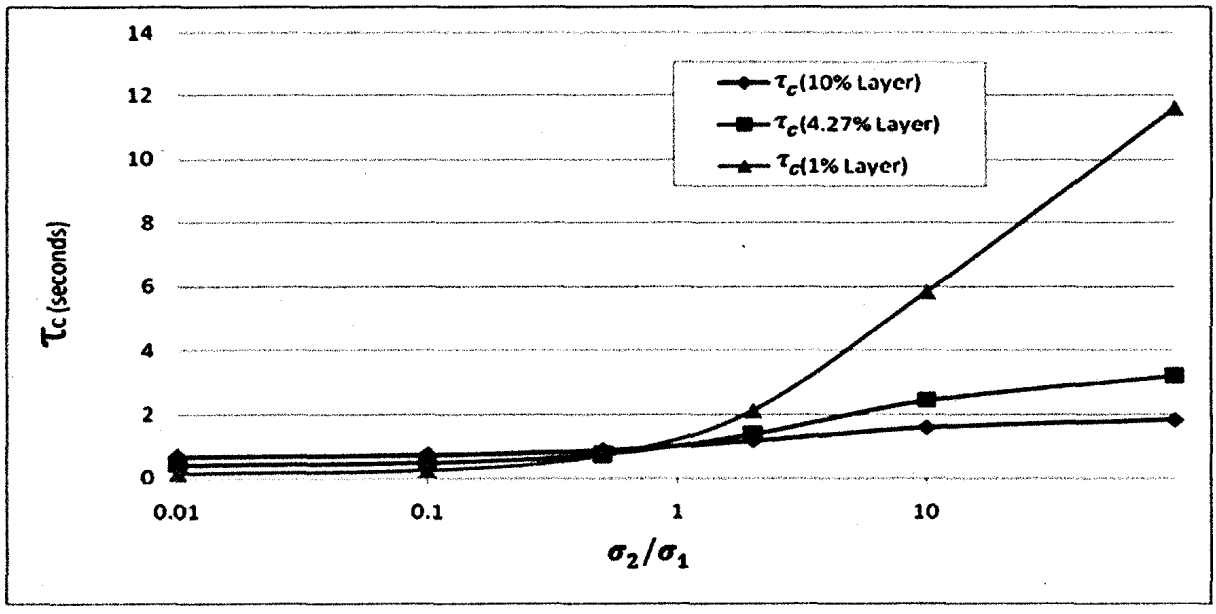

Figure 3.21 The charging time constant for different conductivity ratios and varying surface layer thicknesses for a particle with a 0.039mm² contact area.

From Table 3.7 and Figure 3.21 it can be seen that for a conductivity ratio $\sigma_2/\sigma_1 <$ 1, the charging time constant τ_c increases as the surface layer thickness increases. In this case, a less conducting outer surface layer would result in a slower charging process. When $\sigma_2/\sigma_1 > 1$, the results show that τ_c decreases as the surface layer thickness increases, thus the particle accumulates charge faster with a thicker more conductive outer surface layer.

The results also show that for each layer thickness, τ_c increases as the ratio σ_2/σ_1 increases. The highest increase in the actual charging time constant was shown for the thinnest surface layer of 1%. This also demonstrates the importance of the surface layer thickness on the actual charging time as a thin surface layer results in a smaller effective surface area that directly affects resistance for the charging current. Thinner surface layers would result in a decreased surface conductivity. This in turn will lead to a slower charging process. However, the inner conductivity σ_1 in this case, will have a greater effect, as the surface area is much larger when the surface layer is very thin, and thus a highly conductive inner sphere would result in a much faster charge accumulation process.

3.6.2 Actual charging versus discharging time constant

Theoretically, the actual charging time constant should be equal to the actual discharging time constant, $\tau_c = \tau_d$, as they are directly affected by the electric field, which is identical in both cases. The model used in this section is the spherical particle

with a 4.27% surface layer thickness, assuming particle's relative permittivity equal to 3, σ_2 = 1nS/m, and σ_1 = 0.1nS/m. The spherical particle has a contact area of 0.039mm² with the grounded electrode. The purpose of this simulation is to verify the above intuitive hypothesis by the numerical simulation of the discharging process. Figure 3.22 shows the results when the particle is first charged until the saturation is reached and then it is discharged, assuming that the external electric field has been removed.

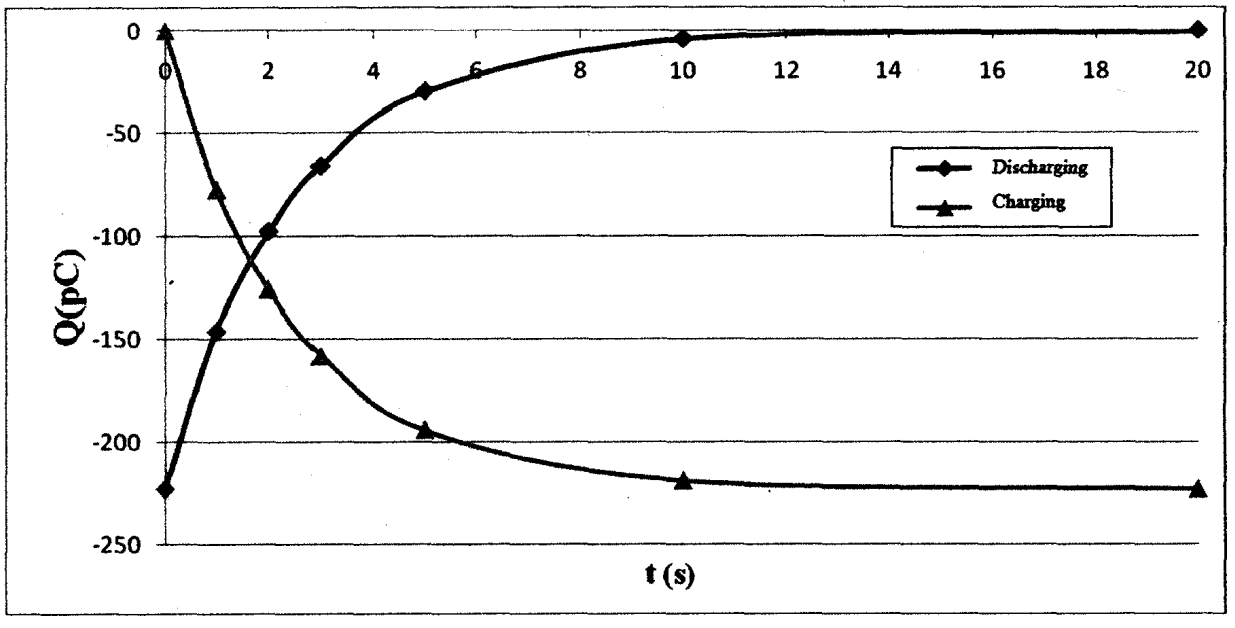

Figure 3.22 Charging versus discharging for a particle with 4.27% layer thickness, constant permittivity and conductivity ratio, and a 0.039mm² contact area with the ground.

As expected, the actual charging and discharging time constants are equal, with $\tau_c = \tau_d$ = 2.42 seconds as shown from Table 3.7 in the previous section. Figure 3.22 shows that both the exponential increase (charging) and exponential decrease (discharging) are horizontally symmetric. These results show that for the particle exposed

to a uniform electric field, the discharging process is the exact reverse of the charging process, assuming the field has been removed upon discharging.

3.7 Summary

A model for investigating the dynamics of induction charging for particles with finite conducting surface layer has been developed. Two-dimensional modelling using COMSOL commercial software was used to geometrically represent two concentric spheres: an inner sphere representing the bulk particle and an outer sphere representing the surface layer. The first step was to verify the model's validity and accuracy. The results of saturation charge obtained for a sphere with a point contact and a hemisphere were validated with analytical calculations from Felici's formulae [2] of a sphere and a hemisphere. The results were proven to be valid and accurate. Following this, the process was simulated for different surface layer thicknesses, volume conductivities and permittivities to compare saturation charge and actual charging time constants. The conclusions can be summarized as follows.

The spherical particle with a finite contact area with the grounded electrode was modelled. For a fixed surface layer thickness and permittivity, an outer volume conductivity greater than an inner volume conductivity ($\sigma_2 > \sigma_1$) resulted in a faster charging process. The surface charge density on the outer sphere, where all the charge resides, showed that volume conductivity had a direct effect on the actual charging time constant. Increasing σ_2 would significantly decrease the actual charging time and results in faster accumulation of charge. Saturation charge is independent of the volume

conductivity, as the particle accumulates the same amount of charge after some period of time, regardless of conductivity changes. Surface charge density for the inner sphere (outer surface of Region 1) was shown to disappear after a short period of time. Theoretically, all charges reside on the surface of a conductor with no charge inside the particle when the charge saturates.

For a finite contact area with the ground, finite surface layer thickness and fixed volume conductivities, accumulation of charge was only slightly faster for particles with higher permittivity. Upon varying both volume conductivities and the permittivity of the particle, it was shown that the volume conductivity had a much greater effect than permittivity on the actual charging time constant. Particles having $\sigma_2 > \sigma_1$ showed faster accumulation of charge even with a decreased permittivity.

The effect of varying contact areas with the ground was also studied. Particles with point contact with the ground showed very slow charging process when compared to particles with finite contact areas. Increasing the contact area however resulted in a smaller contact resistance with the grounded electrode. This in turn led to a faster charge flow, and, therefore, the charging process was faster. The hemisphere was shown to have the fastest charging, because it has the largest contact area with the ground. When compared to the relaxation time constant which depends on the bulk material properties, the actual charging time constant was significantly greater. As the contact area of the particle with the ground gets smaller the actual charging time constant increases. This has shown that the charging rate is related directly to the contact area of the particle with the ground.

The surface layer was created in this model geometrically by adding a concentric second sphere. It was also necessary to introduce three other spherical surfaces for the charge integration. All these factors created a geometric limitation in the COMSOL software that restricted modeling very thin layer thicknesses; a 1% surface layer thickness was the minimum that could be achieved. Upon studying the effect of the surface layer thickness several findings were shown. For particles with $\sigma_2 > \sigma_1$, decreasing the surface layer thickness resulted in a slower accumulation of charge. This was due to surface conductivity which is directly proportional to the outer volume conductivity (σ_2) and the surface layer thickness. As the surface layer thickness and surface conductivity had a critical effect on the actual charging time constant, alternative ways of modelling the surface layer were investigated to get very thin surface layers. This will be discussed in the next chapter.

Discharging of the particles was also simulated and compared to the charging process. The results showed that both the charging and discharging graphs were horizontally symmetric showing that the actual charging and discharging time constants are equal, for particles exposed to a uniform electric field.

Chapter 4
Dynamics of Induction Charging of Multiple Particle Agglomerations

4.1 Introduction

In the previous chapter, the dynamics of induction charging for spherical particles was studied using two-dimensional models in the COMSOL commercial software. The surface layer of the particle was represented by an outer sphere, and geometric limitations of the COMSOL software prevented reducing the surface layer thickness below some critical value. The surface layer with the thickness equal to 4.27% of the particle radius was the least achievable limit to investigate accumulation of the surface charge densities on both the outer sphere (the surface layer), and the inner sphere (the bulk particle). A 1% surface layer thickness was achieved upon simplifying the geometry of the model, by removing the inner artificial integration surfaces and calculating the total charge on the surface of the particle only.

The results presented in Chapter 3 showed that the surface conductivity, which is directly related to the surface layer thickness and volume conductivity, has a major effect on the actual charging time constant of the spherical particle. An alternative way of representing the surface layer of the particle is to reduce the thickness of the layer to a very low value and use a lumped model of this layer. In this technique there is no theoretical limit on the layer thickness; for example particles with about a 20 Å moisture layer thickness can be simulated. This option is also available in COMSOL.

Only single spherical particles were simulated in the previous chapter. In electrostatic applications, particles are typically stacked in an arbitrary array. Upon exposure to the electric field, electric shielding can occur due to the proximity of other particles. Electric shielding can be the result of contact surfaces of multiple particles, shielding the electric field from other particles in a certain pattern. This can greatly reduce the saturation charge of the particles from the value of a single particle. The actual charging time constant and charging process dynamics will also be affected, as a particle loses charge in favour of other particles that are in contact with it. In this chapter, three-dimensional modelling is introduced for the simulations conducted, to model charging of multiple spherical particles in various patterns having very thin surface layer thicknesses.

4.2 Mathematical Model

The mathematical model used for the basic single spherical particle was the same as described in Chapter 3 for two-dimensional modelling. However, the surface conducting layer with finite thickness doesn't need to be defined; it is incorporated using an Electric Shielding boundary condition, available in COMSOL, specifying all the parameters of surface layer: thickness (d), volume conductivity (σ_2) and permittivity (ε_2). Figure 4.1 illustrates the geometrical representation for the model.

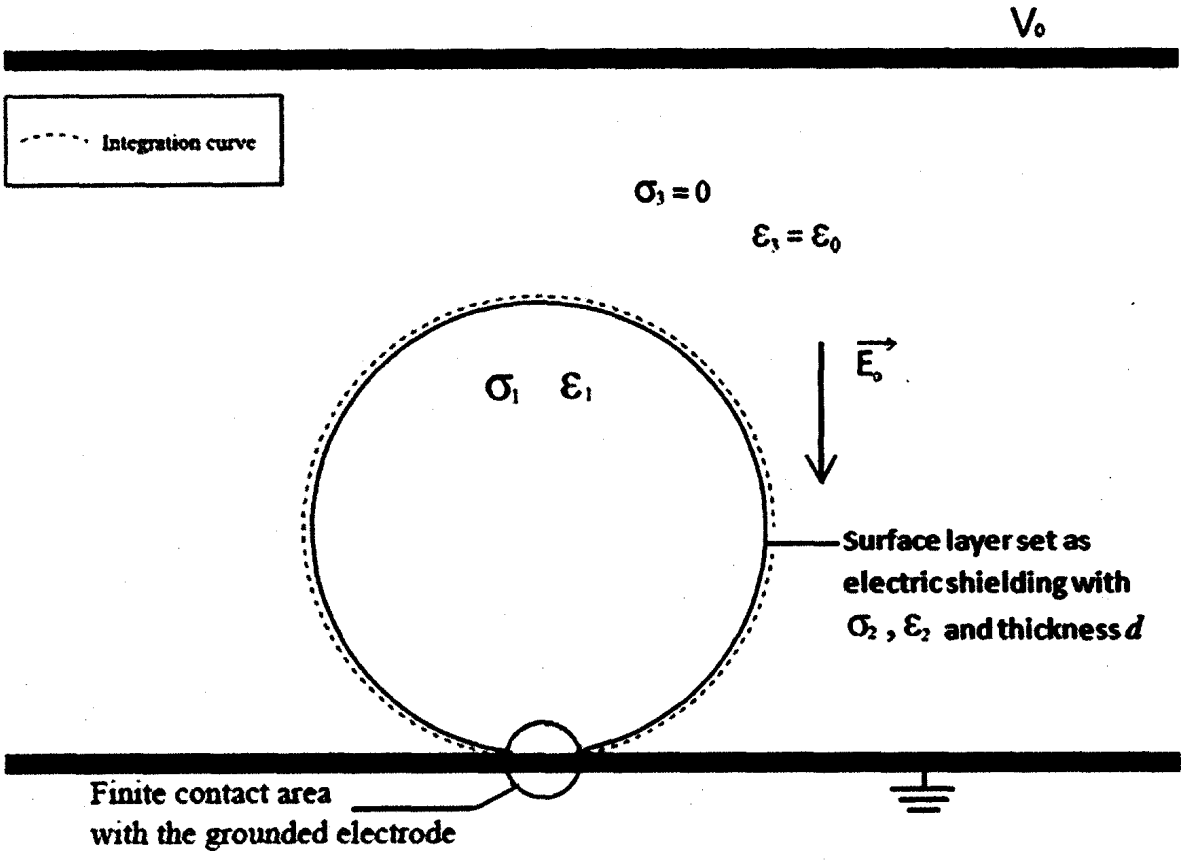

Figure 4.1 Conducting spherical particle with surface layer represented as an electric shield, resting on a grounded electrode and exposed to an external electric field.

The distance between the charging electrodes was also reduced to 0.01m which for the particle sizes studied would have no effect on the results, and enhances memory efficiency when using three-dimensional modelling. The DC voltage applied on the upper electrode in this case was 5kV, so that the same electric field magnitude of 0.5MV/m was produced as the previous chapter. Firstly, the particle was modelled as a stand-alone sphere with a radius of 1.564mm and the surface layer thickness was varied for different simulations. For most simulations, the surface layer thickness was chosen to be 20 Å with values of surface conductivity reported in practical applications upon exposure of particles to moisture. Surface conductivity can be effectively altered by absorption of

moisture on the surface of the particles [21] [22]. Therefore a moisture layer was simulated to investigate its effect on the dynamics of the charging process for the particles. The outer volume conductivity, σ_2, was varied with the surface layer thickness, d, to compare different values of the surface conductivity, σ_s. The permittivity value of the surface layer, ε_2, was assumed to be constant with $\varepsilon_{r2} = 3$. According to Gauss' law, the total charge accumulated on the spherical particle will be equal to the integral of the normal electric displacement D_n at the surface:

$$Q_s = \iint \rho_s \, ds = \iint D_n \, ds \tag{4-1}$$

where ρ_s is the surface charge density, D_n the normal component of electric displacement and Q_s the total saturation charge. The charging time constant τ_c was evaluated using equation (3-15).

4.3 Simulation Model

The simulation model was created using three-dimensional modelling on the COMSOL commercial software. Two electrodes were represented by horizontal rectangles of 0.05m square and a separation of 0.01m. The lower electrode was grounded, while the upper electrode was supplied with 5 kV, which generates the same electric field magnitude of 0.5 MV/m as the previous chapter. For the transient case, the voltage supplied was represented as V = 5000 * (t > 0). The vertical sides of the rectangle were set as electric insulators.

Initially, a single spherical particle with 1.564mm radius was modelled as shown in Figure 4.1. The particle had a 0.039mm² contact area with the grounded electrode. The surface layer for the particle was represented as an electric shielding boundary condition on COMSOL. Initially, the surface layer thickness, electrical conductivity and permittivity of the particle were varied for different cases, The air region surrounding the particle is non-conductive ($\sigma_3 = 0$) with permittivity $\varepsilon_3 = \varepsilon_0 = 8.854 \times 10^{-12}$ F/m. The surface layer is defined by three finite parameters: electrical conductivity (σ_2), permittivity (ε_2) and thickness (d). The particle's volume conductivity (σ_1) and permittivity (ε_1) are also defined. To integrate the surface charge density and calculate the total charge magnitude, an artificial spherical surface, concentric with the particle, was drawn.

The model was then extended to simulate multiple spherical particle agglomerations. Different patterns of particles were modelled. Surface layer thickness was set constant at 20 Å, all particles were identical and have point contact with each other. The contact area of the particles with the ground is constant, and set to 0.039mm² in all cases.

Finally, upon modelling the geometry of the problem and defining all parameters, the whole domain was meshed using tetrahedral discretizations on COMSOL for three-dimensional modelling.

The simulations were conducted in the transient mode analysis to study the dynamics of the charging process. The total charge accumulated by the particle and actual charging time constant were calculated for the different simulations.

4.4 Model Verification

The first step in this part was to verify the accuracy of the new three-dimensional model, by comparing the results with those obtained from the equivalent two-dimensional model that was previously investigated and verified. In order to achieve this, the charge build-up for both the two-dimensional and three-dimensional models was compared. The results shown in Table 4.1 and Figure 4.2 were conducted for a particle with a 1.564mm radius and 0.01564mm surface layer, i.e. 1% of the radius. Inner and outer conductivities (σ_2 and σ_1) were set to 0.1nS/m and 1nS/m, respectively. The equivalent surface conductivity (σ_s) was 1.564×10^{-14} S/square. The relative permittivity of the particle (ε_r) was set to 3. The particle had a finite contact area of 0.039mm² with the grounded electrode. The results of calculations for the saturation charge agree with the two-dimensional simulations with error of 0.001%.

Table 4.1 Comparison between the results of the 2D and 3D models for a single spherical particle with 0.039mm² contact area

Particle Shape	Induction Charge Q(pC) (2D Model)	Induction Charge Q(pC) (3D Model)	Percentage Difference (%)
Sphere (a = 1.564mm, d = 0.01564mm)	-223.510	-223.513	0.001%

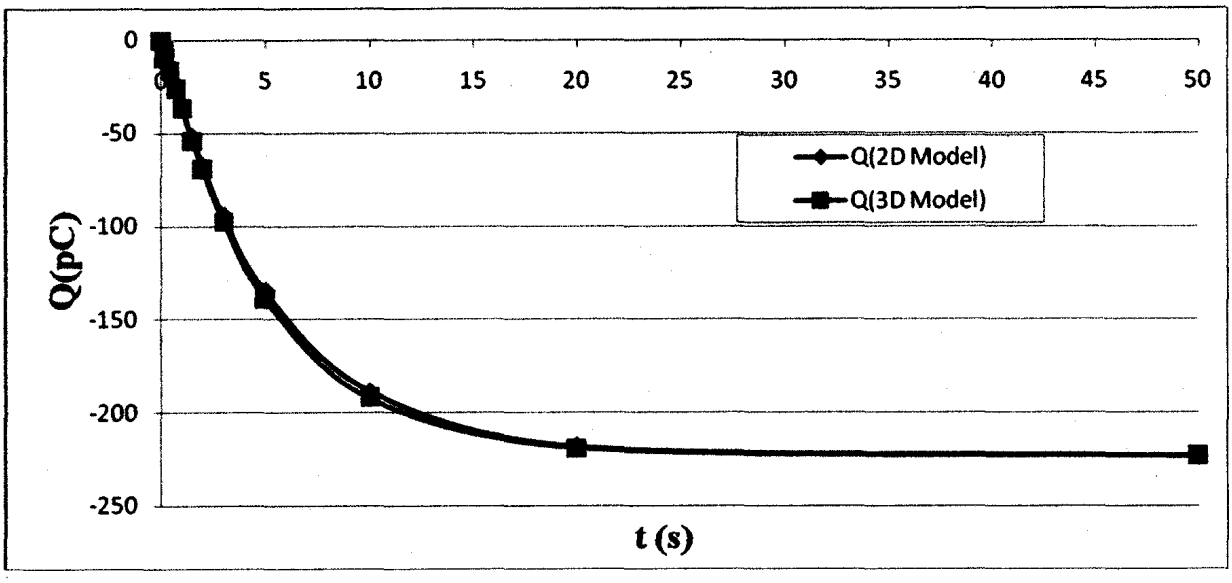

Figure 4.2 Induction charge Q versus time t for the particle having 1% surface layer thickness assuming $\sigma_1 = 0.1$nS/m, $\sigma_2 = 1$nS/m, $\varepsilon_r = 3$.

The charge build up for both the two-dimensional and three-dimensional models (Figure 4.2) is almost identical, with the maximum error at $t = 10$s equal to 1.53%. The results have proven that the three-dimensional model was valid. Following this, a very thin surface layer was simulated to investigate the effect of the surface conductivity. Different particle arrays were also simulated to investigate the effect of electric shielding on the charge build up and saturation charge.

4.5 Single spherical particle in three-dimensional modelling

A single 3D spherical particle was simulated. In all cases, the radius of the sphere was set to 1.564mm assuming a contact area of 0.039mm² with the ground electrode. By defining the surface layer thickness (d) and its conductivity (σ_2), the equivalent surface conductivity (σ_s) can be obtained.

In the previous chapter, a limitation on the surface layer thickness equal to 1% of the particle radius was caused by the internal restrictions of COMSOL. By implementing the new method of specifying the thickness as a parameter in three-dimensional modelling, negligibly thin surface layers could be achieved. Simulations were conducted assuming surface layer thicknesses of 4.27%, 1% and 10^{-8} % of the particle radius. The parameters were set as: σ_1 = 0.1nS/m, σ_2 = 1nS/m and ε_r = 3. The plots of the induction charge Q as a function of time t for the particles with increasing surface layer thicknesses are shown in Figure 4.3.

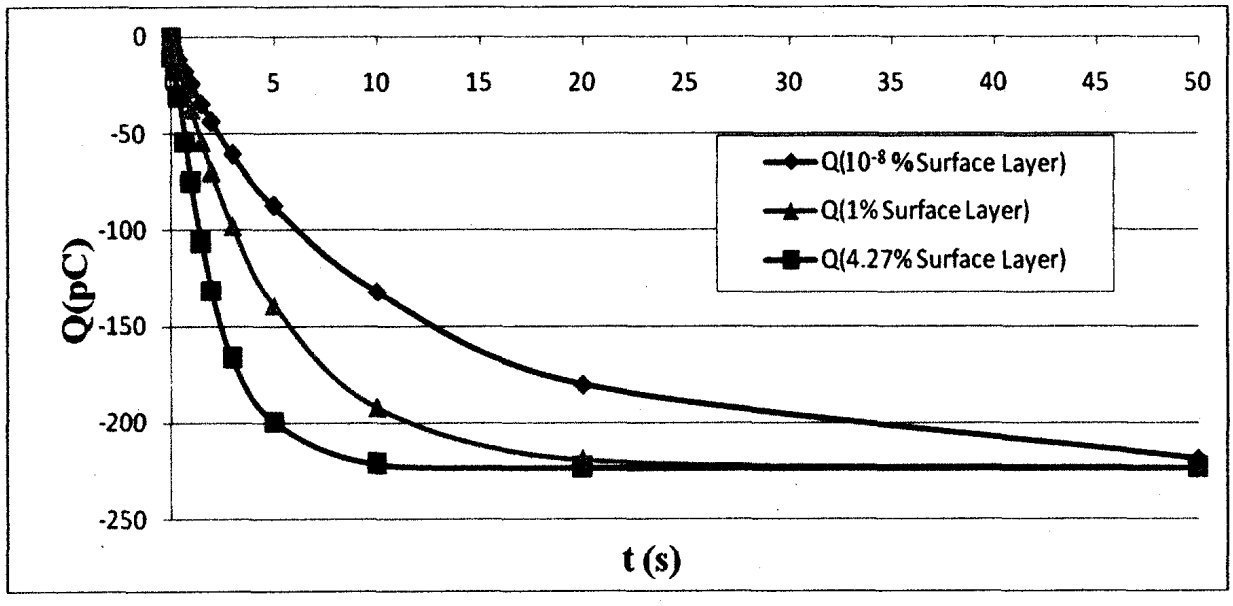

Figure 4.3 Induction charge Q versus time t for the particle having different surface layer thicknesses assuming σ_1 = 0.1nS/m, σ_2 = 1nS/m, and ε_r = 3.

Further simulations were done to study the effect of the 10^{-8}% surface layer when varying the conductivity ratios between the particle and its surface layer. Table 4.2 summarizes the results showing the actual charging time constants for two different ratios.

Table 4.2 Actual charging time constants for varying conductivity ratios

σ_2/σ_1	10	100
τ_c(s) 4.27% Layer	2.4	3.2
τ_c(s) 1% Layer	5.75	11.5
τ_c(s) 10^{-8}% Layer	14.3	114.6

It can be seen from Figure 4.3 and Table 4.2, when the surface layer thickness is decreased and keeping the conductivity ratio of $\sigma_2/\sigma_1>1$, the charge accumulation on the particle was slower. These results were presented in the previous chapter, but in this section they are confirmed for a very thin surface layer. The results also show that after decreasing the surface layer thickness (σ_s decreases for fixed volume conductivity), the actual charging time constant (τ_c) has increased. A significant increase in τ_c for σ_2/σ_1 = 100 was shown for the particle having 10^{-8} % surface layer thickness, with a value of 114.6 seconds. It can be concluded that surface conductivity affects the actual charging time constant significantly; a decreased surface conductivity resulted in a slow charging process.

Further simulations were conducted using practical values of surface layer thickness to investigate this effect. The surface layer thickness was set to 20 Å. The outer volume conductivity (σ_2) was set to 0.005S/m, which is between the tap water conductivity of 0.01 S/m and fresh water conductivity of 0.001 S/m. This would represent moisture layer parameters. Surface conductivity σ_s was then calculated to be 10^{-11} S/square. The particle's relative permittivity was set to ε_r= 3. The plot for the induction charge Q versus time t is shown in Figure 4.4 and the results summarized in Table 4.3.

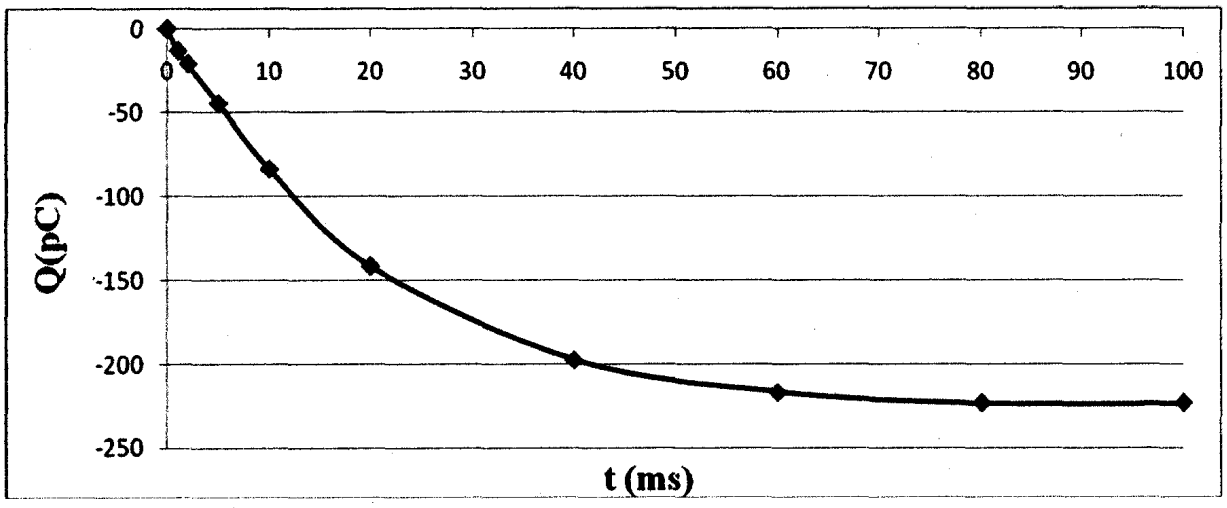

Figure 4.4 Induction charge Q versus time t for the particle with $\sigma_2 = 0.005$S/m, $\sigma_1 = 0.1$nS/m, $\varepsilon_r = 3$, $d = 20$ Å and $\sigma_s = 10^{-11}$ S/square.

Table 4.3 Charging dynamics of particle with 20 Å surface layer thickness and 10^{-11} S/square surface conductivity.

Particle Shape	Saturation Charge Q_s(pC)	Actual Charging Time Constant τ_c(ms)	Relaxation Time Constant τ_r(s) ($\tau_r = \varepsilon_1/\sigma_1$)	τ_c/τ_r
Particle with 20 Å Surface Layer Thickness (σ_s= 10^{-11} S/square)	-223.51	20	0.266	0.08

From Table 4.3 it can be seen that for a thin layer of 20 Å, with a surface conduction of 10^{-11} S/square, the charging time constant (τ_c) was 20ms. When compared to previous results, it is clearly shown that a higher surface conductivity results in a much faster charge build up. Saturation charge for the spherical particle was -223.51pC as verified earlier. The relaxation time constant (τ_r) of the bulk particle was calculated to be 0.266 seconds, with τ_c/τ_r of 0.08. It can be seen that τ_r is significantly greater than τ_c. In this case the current that flows to charge the particle passes almost entirely through the

thin surface layer due to its higher effective conductivity. In other words the particle properties are effectively shielded by the presence of the outer conductive layer.

From Figure 4.4 it can be seen that charge accumulation is very fast. When compared to the previous cases of lower surface conductivity, the induction charge increases much more rapidly. Two factors directly affect surface conductivity and will affect charge build up: surface layer thickness (d), and outer volume conductivity (σ_2). To investigate the relation between σ_s, σ_2, and d where $\sigma_s = \sigma_2 d$, a simulation was done for particles with different surface layer thickness d and adjusted σ_2 to get the same surface conductivity. Permittivity and inner volume conductivity were fixed: $\varepsilon_r = 3$, $\sigma_1 =$ 0.1nS/m for all cases. Figure 4.5 shows the results for the simulation.

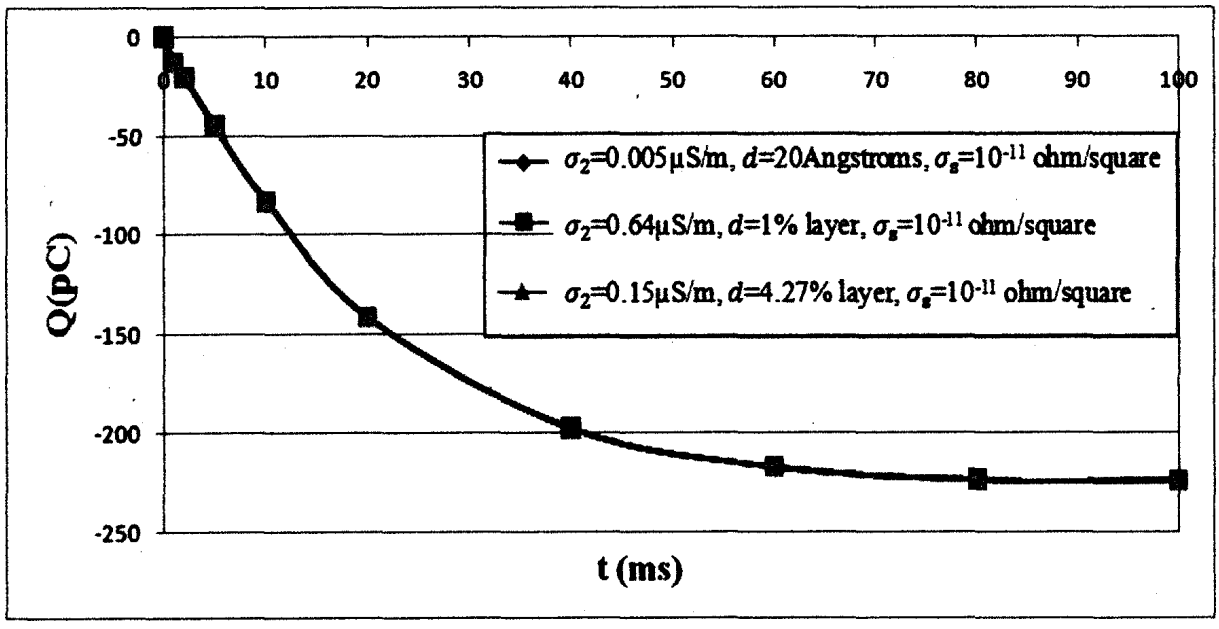

Figure 4.5 Induction charge Q versus time t for particles with varying σ_2 and d, and fixed σ_s.

From Figure 4.5 for particles with the same surface conductivity, regardless of the layer thickness and outer volume conductivity, it is shown that all curves coincide and the charging process is the same. τ_c was equal to 20ms for all cases, assuming $\sigma_s = 10^{-11}$ S/square. It is shown that $\sigma_s = \sigma_2 d$ is in excellent agreement with the simulation results and the charging dynamics for the particle are directly affected by its surface conductivity.

4.6 Multiple particle agglomerations

Multiple particle arrays were simulated to investigate the charging dynamics in agglomerations of particles, and the effect of electric shielding on the particles' actual charging time constant and saturation charge. All particles were assumed to be spherical with a radius of 1.564mm, a surface layer of thickness $d = 20$ Å and surface conductivity $\sigma_s = 10^{-11}$ S/square, which corresponds to 0.005 S/m volume conductivity in the outer layer. Permittivity and inner volume conductivity were fixed: $\varepsilon_r = 3$, $\sigma_1 = 0.1$nS/m for all cases. The multiple particle agglomerations consisted of five spheres, thirteen spheres and twenty one spheres aligned horizontally. In order to further investigate shielding of the particles, a group of five spheres on top of five other identical spheres was investigated.

4.6.1 Agglomeration of thirteen particle pattern

The geometric representation of the thirteen-particle agglomeration is shown in Figure 4.6. All particles are placed flat on the ground electrode with a symmetrical

arrangement, so that only four particles (numbered as 1, 2, 3 and 4) represent distinct cases.

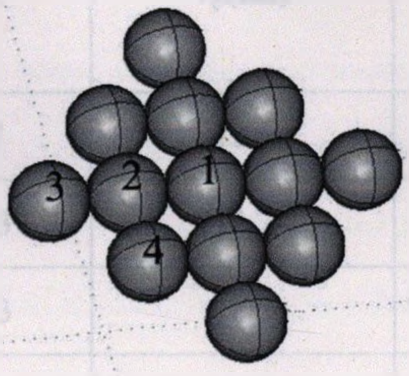

Figure 4.6 Thirteen-particle agglomeration

The charging dynamics were investigated for particles 1-4, and the results summarized in Figure 4.7 and Table 4.4.

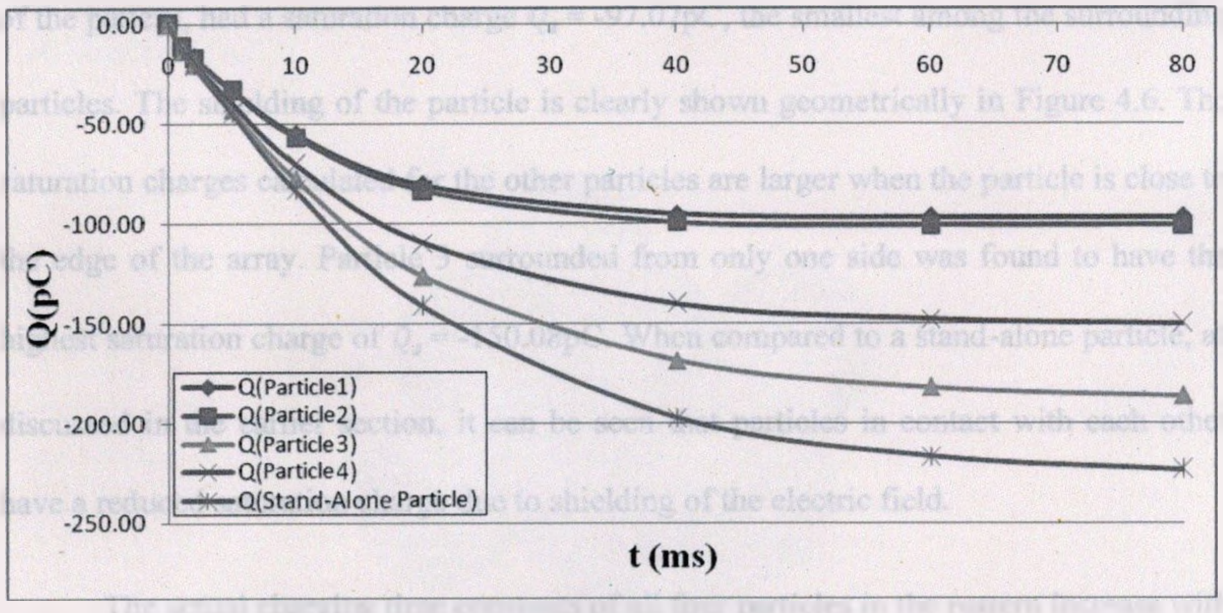

Figure 4.7 Induction charge Q versus time t for the particles 1-4 compared with a stand alone particle assuming $\sigma_2 = 0.005$S/m, $\sigma_1 = 0.1$nS/m, $\varepsilon_r = 3$, $d = 20$ Å and $\sigma_s = 10^{-11}$ S/square.

Table 4.4 Charging dynamics of particles in thirteen particles agglomeration

Particle	Saturation Charge Q_s(pC)	Actual Charging Time Constant τ_c(ms)	Relaxation Time Constant τ_r(s) ($\tau_r = \varepsilon_1/\sigma_1$)	τ_c/τ_r
1	-97.07	12.5	0.266	0.05
2	-101.03	12.7	0.266	0.05
3	-186.33	18.3	0.266	0.07
4	-150.08	16.3	0.266	0.06
Stand-Alone Particle	-223.51	20	0.266	0.08

From Figure 4.7 and Table 4.4 it can be seen that Particle 1, located at the center of the pattern, had a saturation charge Q_s = -97.07pC, the smallest among the surrounding particles. The shielding of the particle is clearly shown geometrically in Figure 4.6. The saturation charges calculated for the other particles are larger when the particle is close to the edge of the array. Particle 3 surrounded from only one side was found to have the highest saturation charge of Q_s = -150.08pC. When compared to a stand-alone particle, as discussed in the earlier section, it can be seen that particles in contact with each other have a reduced saturation charge due to shielding of the electric field.

The actual charging time constants of all four particles in the pattern increase with reduced shielding, but differences are not very large. Particle 3 with the weakest shielding effect has the slowest accumulation of charge with a charging time constant τ_c

= 18.3ms. This is a surprising effect, as the less shielded particles have a higher saturation charge, so it would be intuitively expected that the charging time constant would be higher. A stand-alone particle with no shielding has τ_c = 20ms. The results have also shown that $\tau_c \ll \tau_r$ for all particles. The ratio τ_c/τ_r increases with weaker shielding of the particles. Therefore, the actual charging time constant and saturation charge were found to be directly affected by shielding of the particles, caused by proximity of other particles. Further geometric models will be investigated for different particle patterns to investigate the electric shielding effect on the charging dynamics of the particles.

4.6.2 Five-over-Five particle pattern

The geometric representation of a five-over-five particle pattern is shown in Figure 4.8. The results are presented for the particles 1, 2, 3 and 4 only, due to the symmetric arrangement in the pattern. The results were summarized in Figures 4.9 and 4.10, and Table 4.5.

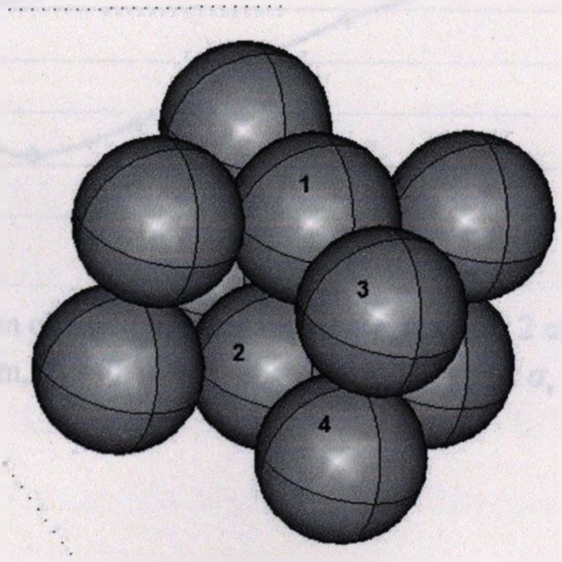

Figure 4.8 Five-over-five particle pattern

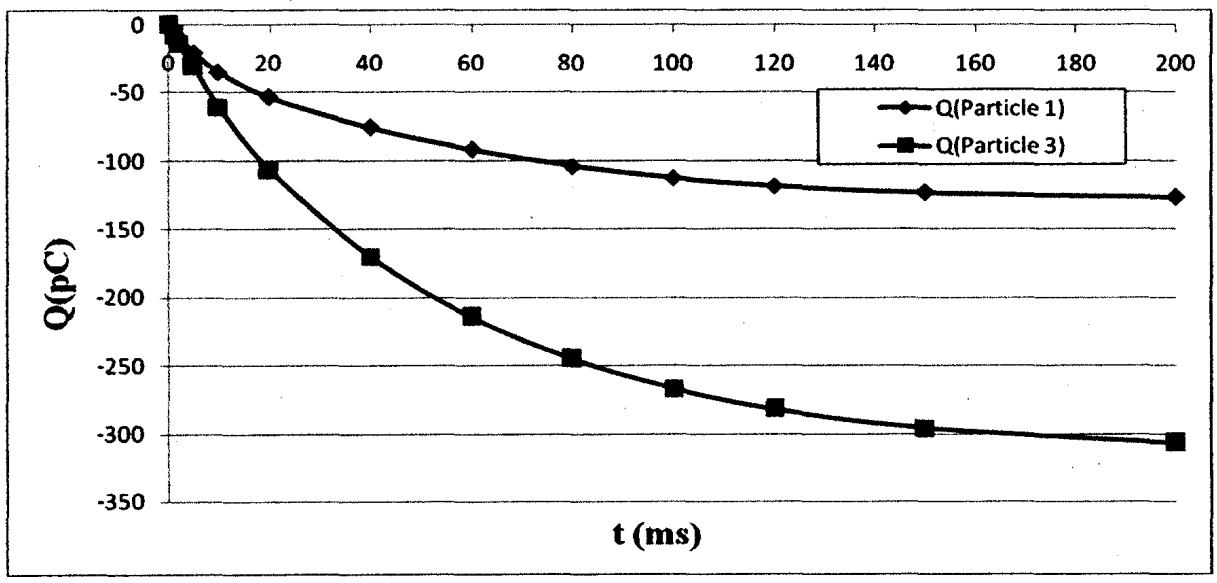

Figure 4.9 Induction charge Q versus time t for particles 1 and 3 assuming σ_2 = 0.005S/m, σ_1 = 0.1nS/m, ε_r = 3, d = 20 Å and $\sigma_s = 10^{-11}$ S/square.

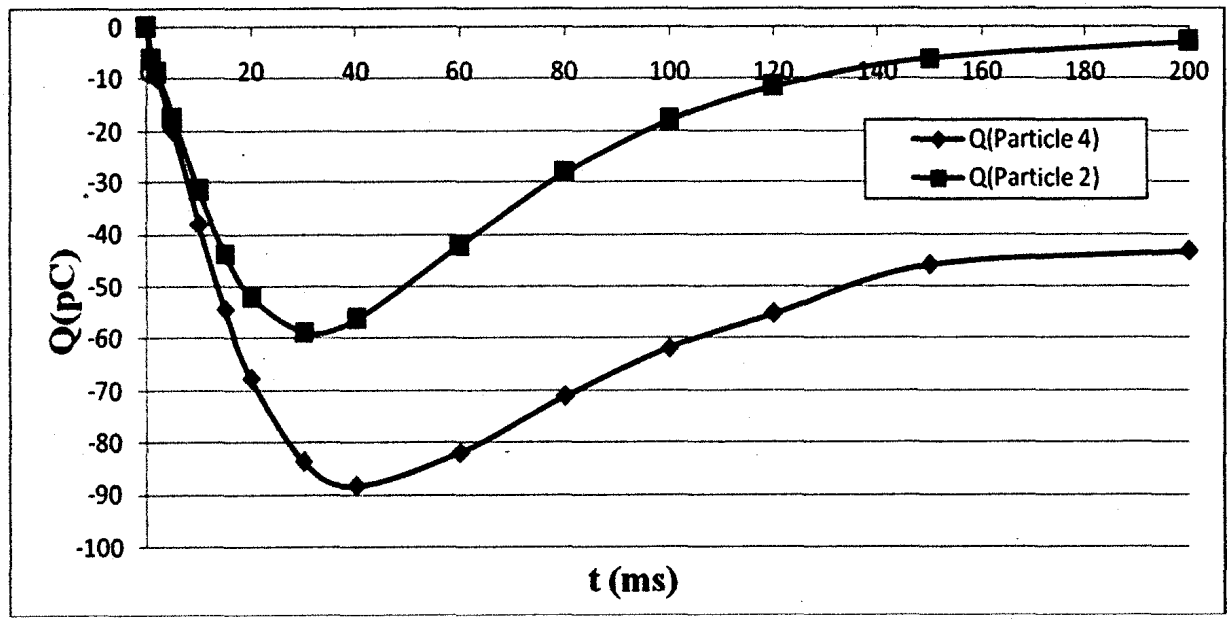

Figure 4.10 Induction charge Q versus time t for particles 2 and 4 assuming σ_2 = 0.005S/m, σ_1 = 0.1nS/m, ε_r = 3, d = 20 Å and $\sigma_s = 10^{-11}$ S/square.

Table 4.5 Charging dynamics of particles in five-over-five particle pattern

Particle	Saturation Charge Q_s(pC)	Actual Charging Time Constant τ_c(ms)	Relaxation Time Constant τ_r(s) ($\tau_r = \varepsilon_1/\sigma_1$)	τ_c/τ_r
1	-126.77	42.4	0.266	0.16
3	-310.98	53.6	0.266	0.20

As it can be seen from Figure 4.9 and Table 4.5, Particle 3 is not shielded by other particles and reaches the highest saturation charge Q_s = -310.98pC. The actual charging time constant τ_c was also the largest for Particle 3, even though it acquires more charge than Particle 1. τ_c/τ_r increases with less shielding of the particles, as τ_c increases. It can also be noted that Particle 3 has a saturation charge Q_s greater than that of a stand-alone particle. This was due to elevation of Particles 1 and 3, which would be exposed to a stronger electric field.

Particles 2 and 4, shielded from the top by Particles 1 and 3, are exposed to a smaller electric field. From Figure 4.10 it can be seen that the charge accumulates in the beginning then decays. As the current initially flows from the ground plate to the lower particle, the charge builds up. The electric field directed downward from the upper electrode is mainly blocked, shielding Particles 2 and 4. The shielded particles are still exposed to some electric field, and this is shown as they accumulate some charge. The loss of charge noticed in Figure 4.10, is the result of charges moving from the lower shielded particles to the upper residing ones, i.e. Particles 2 and 4 lose charge in favour of

1 and 3. Moreover, Particle 2, shielded from all sides, is seen to lose charge almost entirely upon saturation.

It can be concluded, that the particles in the top layer acquire more charge than those in contact with the grounded electrode, because of exposure to a stronger electric field. Particles in the lower layer experience much weaker electric field, because they are shielded by the electric charge accumulated in the top layer. In the first phase, the charge increases rather quickly, because the upper layer is not charged yet. However, the charge accumulation in the upper layer decreases the electric field in the area below, reducing the electric charge of Particles 2 and 4.

4.6.3 Increased electric shielding on the central particle

To further investigate the effect of shielding a spherical particle, multiple particle agglomerations were modelled, and the results were compared for the central particle, which will be the most shielded. The saturation charge, charging dynamics and the actual charging time constant for different cases were compared. Figures 4.11(a), 4.11(b) and 4.11(c) show three different geometric models that were investigated.

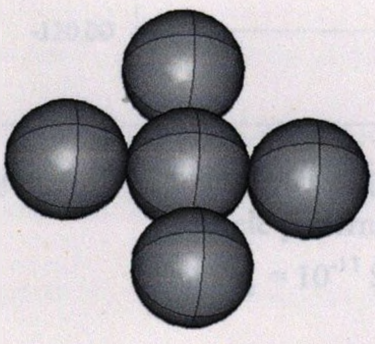

Figure 4.11(a) Five-particle agglomeration

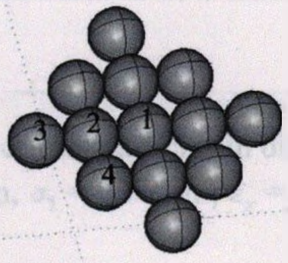

Figure 4.11(b) Thirteen-particle agglomeration

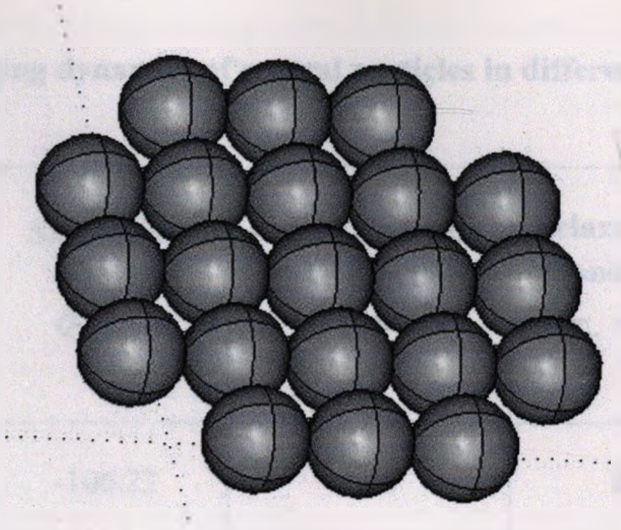

Figure 4.11(c) Twenty one particle agglomeration

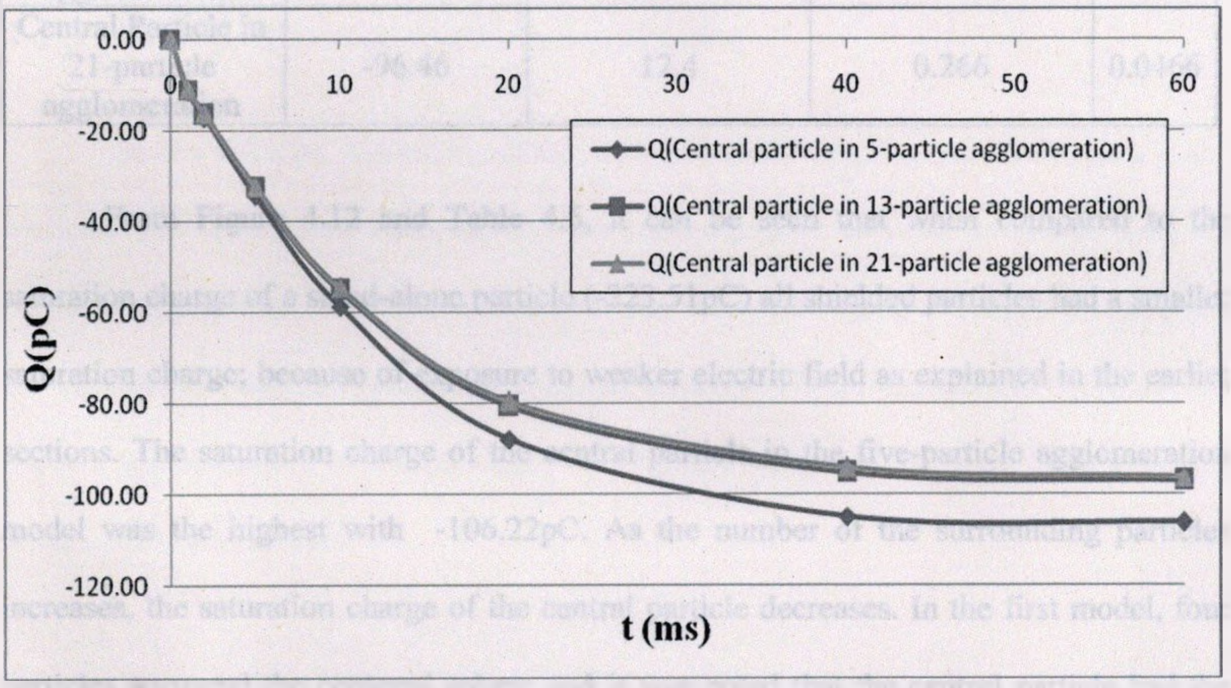

Figure 4.12 Induction charge Q versus time t for the central particles in different particle patterns assuming $\sigma_2 = 0.005$S/m, $\sigma_1 = 0.1$nS/m, $\varepsilon_r = 3$, $d = 20$ Å and $\sigma_s = 10^{-11}$ S/square.

Table 4.6 Charging dynamics of central particles in different particle agglomerations

Particle	Saturation Charge Q_s(pC)	Actual Charging Time Constant τ_c(ms)	Relaxation Time Constant τ_r(s) ($\tau_r = \varepsilon_1/\sigma_1$)	τ_c/τ_r
Central Particle in 5-particle agglomeration	-106.22	12.8	0.266	0.0481
Central Particle in 13-particle agglomeration	-97.07	12.5	0.266	0.047
Central Particle in 21-particle agglomeration	-96.46	12.4	0.266	0.0466

From Figure 4.12 and Table 4.6, it can be seen that when compared to the saturation charge of a stand-alone particle (-223.51pC) all shielded particles had a smaller saturation charge; because of exposure to weaker electric field as explained in the earlier sections. The saturation charge of the central particle in the five-particle agglomeration model was the highest with -106.22pC. As the number of the surrounding particles increases, the saturation charge of the central particle decreases. In the first model, four particles surround the centered sphere and it was noted that the central particle had the highest saturation charge and highest actual charging time constant τ_c among the other models. τ_c/τ_r decreased when increasing the number of surrounding particles, due to an increase in τ_c.

It was also shown that increasing the number of surrounding particles from twelve (13-particle agglomeration) to twenty (21-particle agglomeration) will not affect the saturation charge of the central particle. This is shown in Figure 4.12 where the increase in saturation charge Q_s and charging time constant τ_c of the central particle changes only slightly. Therefore, it can be concluded that a particle surrounded by other particles will have a lower saturation charge and actual charging time constant up to a certain point where increased shielding (adding more surrounding particles) on the central particle will have no more effect on its saturation charge and charging process.

4.6.4 Charging versus discharging process

For the different models simulated, a few cases of charging and discharging of the particles were simulated. Theoretically, for a uniform electric field, the actual charging and discharging time constants should be equal. The discharging process was simulated for the thirteen-particle agglomeration model shown in Figure 4.6 and the five-over-five particle agglomeration model of Figure 4.8. Figures 4.13, 4.14, 4.15 and 4.16 show the results of the simulations.

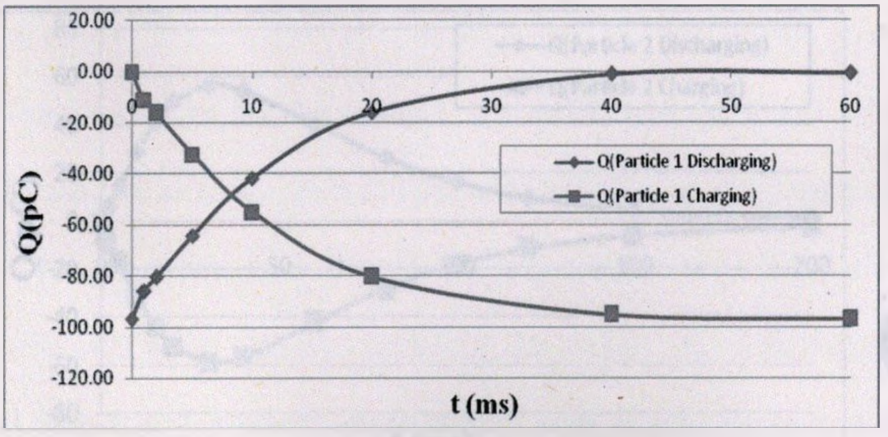

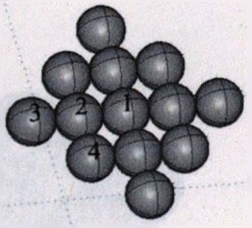

Figure 4.13 Charging versus discharging for Particle 1

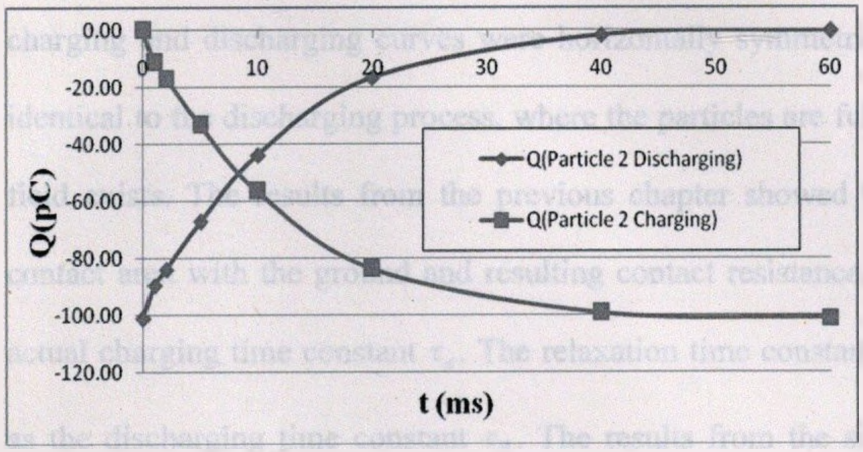

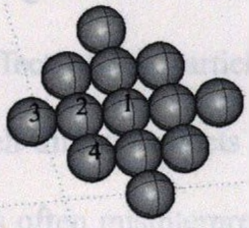

Figure 4.14 Charging versus discharging for Particle 2

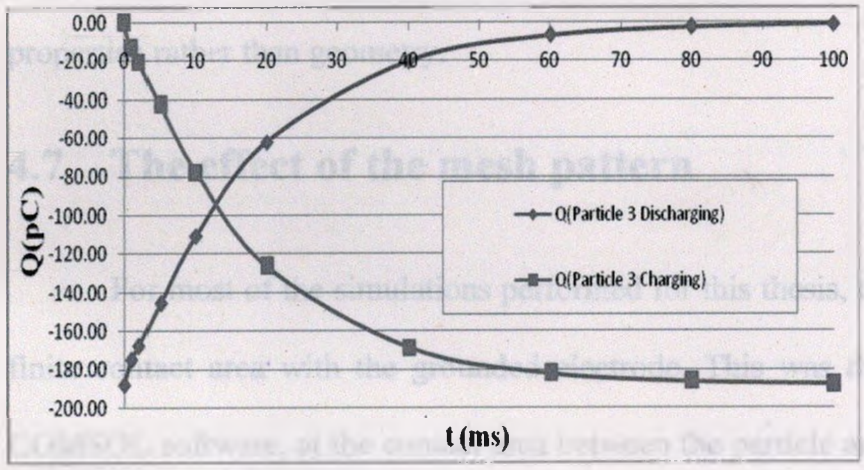

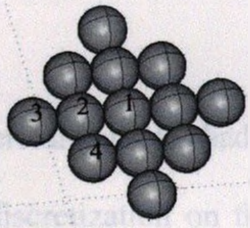

Figure 4.15 Charging versus discharging for Particle 3

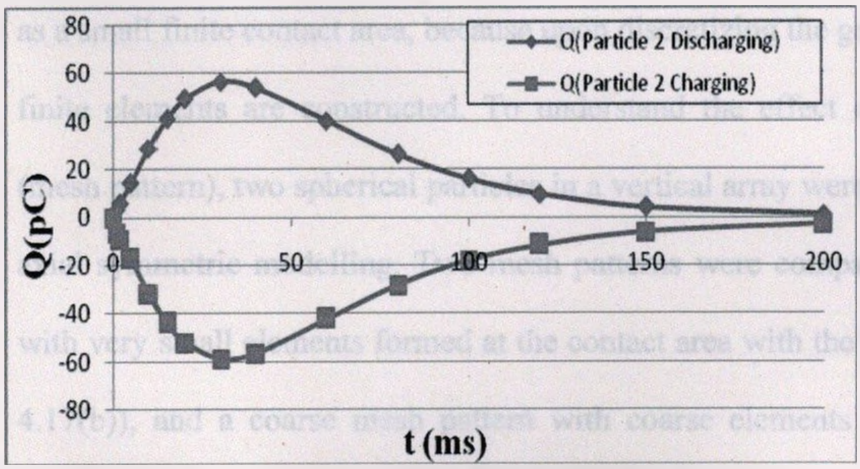

Figure 4.16 Charging versus discharging for Particle 2

As expected, the results shown in Figures 4.13 – 4.16 show that $\tau_c = \tau_d$; the charging and discharging curves were horizontally symmetric. The charging process is identical to the discharging process, where the particles are fully charged and no external field exists. The results from the previous chapter showed the effect of the particle's contact area with the ground and resulting contact resistance, which directly affects the actual charging time constant τ_c. The relaxation time constant τ_r is often misinterpreted as the discharging time constant τ_d. The results from the simulations showed that the actual charging and discharging numerical results are similar, yet different from the analytical relaxation time constant ($\tau_r = \varepsilon/\sigma$), which is directly affected by particle's properties rather than geometry.

4.7 The effect of the mesh pattern

For most of the simulations performed for this thesis, the spherical particles had a finite contact area with the grounded electrode. This was due to discretization on the COMSOL software, at the contact area between the particle and the ground, as explained in the previous chapter. Theoretically, a point contact is effectively treated by COMSOL as a small finite contact area, because upon discretizing the geometrical interface, discrete finite elements are constructed. To understand the effect of the discretization pattern (mesh pattern), two spherical particles in a vertical array were created in two-dimensional axial symmetric modelling. Two mesh patterns were compared, a normal refined mesh with very small elements formed at the contact area with the ground (Figures 4.17(a) and 4.17(b)), and a coarse mesh pattern with coarse elements formed at the contact area

(Figures 4.18(a) and 4.18(b)). Particle 2 had a point contact with the grounded electrode, and a point contact with Particle 1.

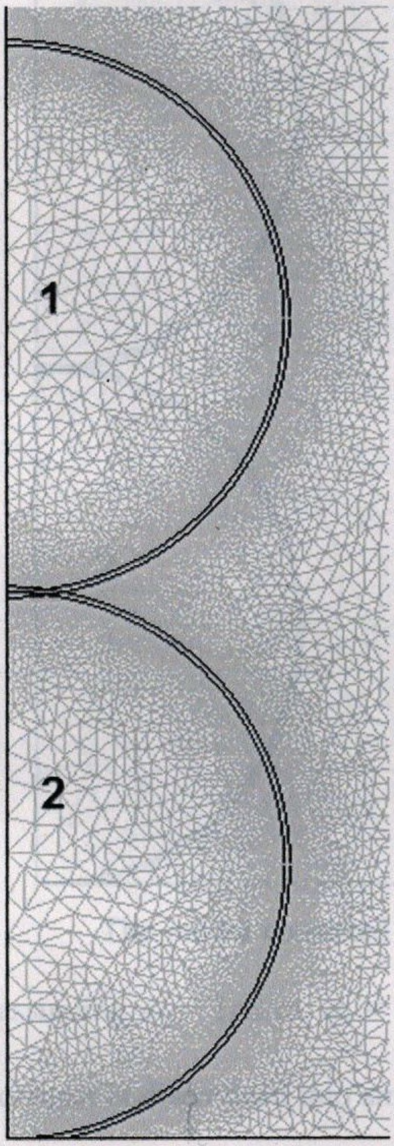

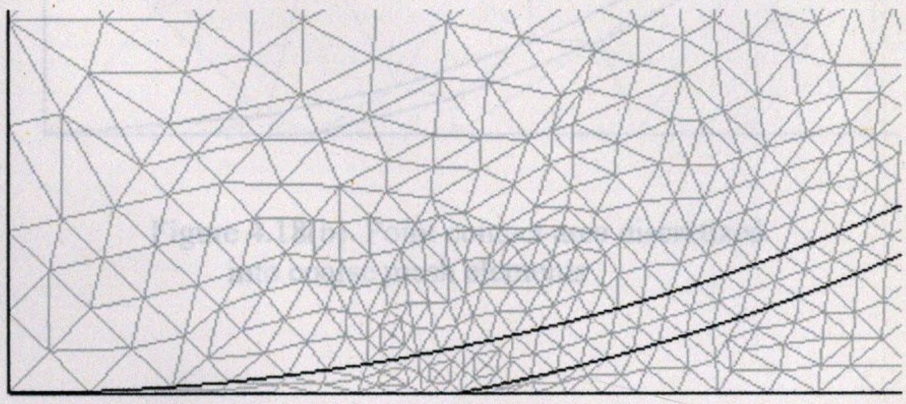

Figure 4.17(b) Point contact area discretized into refined mesh elements

Figure 4.17(a) Refined mesh pattern (Full scale view)

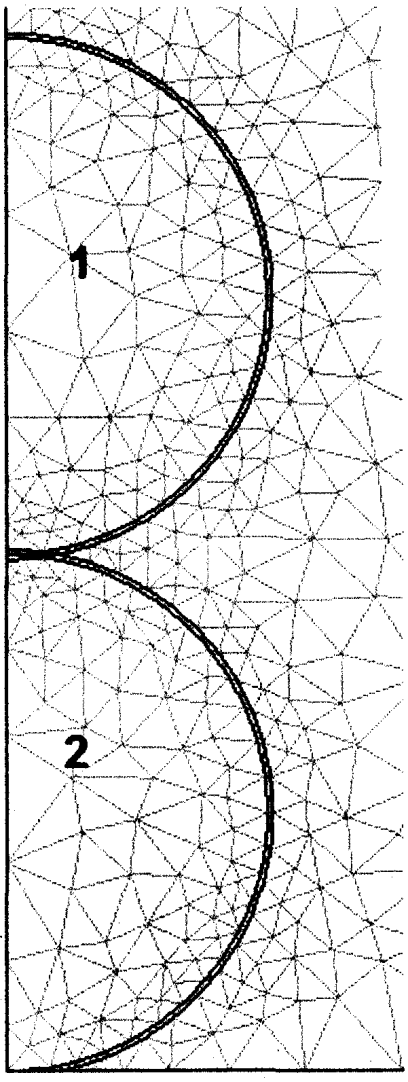

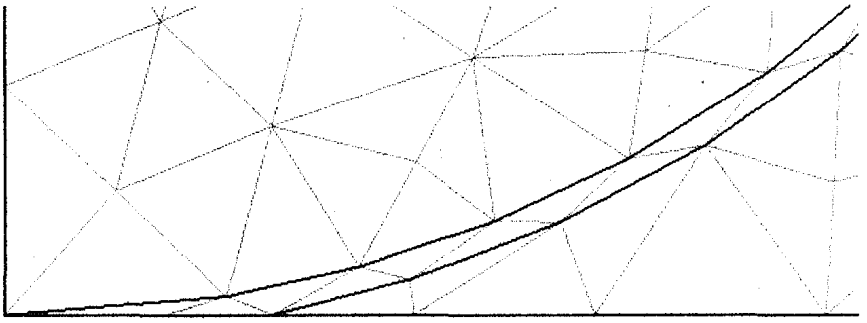

Figure 4.18(b). Point contact area discretized into coarse mesh elements

Figure 4.18(a) Coarse mesh pattern (Full scale view)

The model consisted of two spherical particles of identical radius a = 1.564mm, assuming σ_2 = 1nS/m, σ_1 = 0.1nS/m, ε_r = 3, and 1% surface layer thickness. The point contact is discretized into small finite elements upon meshing the domain. The results of simulation are shown in Figures 4.19, 4.20 and Table 4.7.

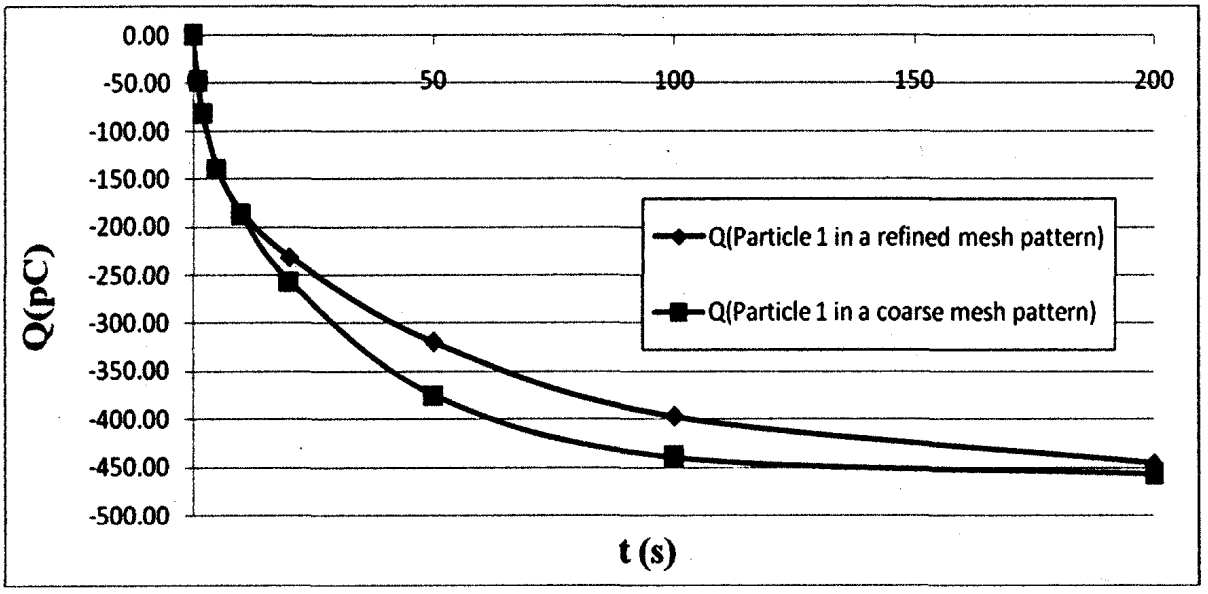

Figure 4.19 Induction charge Q versus time t for Particle 1 in a refined and coarse mesh pattern

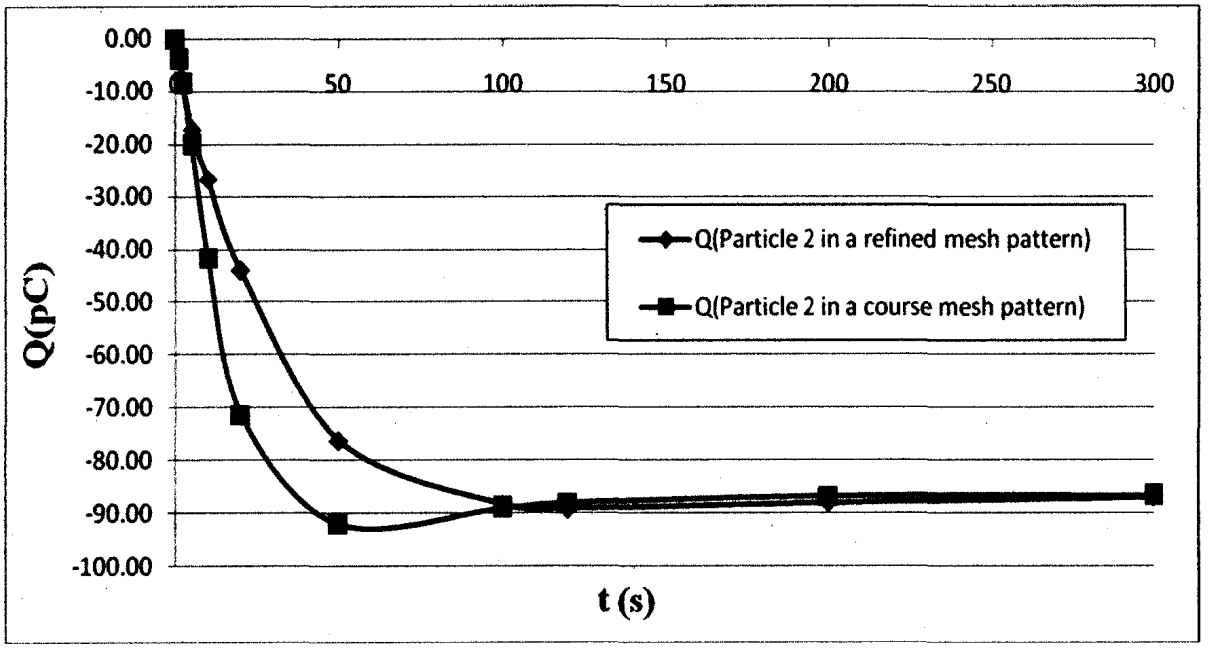

Figure 4.20 Induction charge Q versus time t for Particle 2 in a refined and coarse mesh pattern

Table 4.7 Charging dynamics for the particles in a two particle vertical arrangement for refined and coarse mesh patterns

Particle	Saturation Charge Q_s(pC)	Actual Charging Time Constant τ_c(s)	Relaxation Time Constant τ_r(s) $(\tau_r = \varepsilon_1/\sigma_1)$	τ_c/τ_r
Particle 1 (Refined Mesh)	-457.8	39.6	0.266	148.87
Particle 1 (Coarse Mesh)	-457.92	28.3	0.266	106.39
Particle 2 (Refined Mesh)	-86.71	30.1	0.266	113.16
Particle 2 (Coarse Mesh)	-86.66	14.4	0.266	54.14

It can be seen from Table 4.7, that the saturation charge for the particles having a refined mesh is only slightly smaller than that for the case of a coarse mesh. Particle 1 elevated on top of particle 2 was shown to have a high saturation charge of -457.8pC for a refined mesh and -457.92pC for a coarse mesh. As particle 1 is closer to the upper charged electrode, a resulting high saturation charge would be expected. Particle 2 shielded by particle 1 would be exposed to a smaller electric field and its saturation charge is reduced. The results are in perfect agreement with previous simulations conducted for multiple particle agglomerations: elevated particles accumulate more charge, and shielded particles have a reduced saturation charge depending on the intensity of the electric shielding.

From Figures 4.19 and 4.20 it is shown that charge accumulation was slower for a refined mesh. An equivalent finite contact area to a point contact, introduced by the

COMSOL software, is larger for a coarse discretization and smaller for a fine discretization. This would show that for a smaller contact area with the ground (as in the case of the refined mesh with finer discretizations), the contact resistance increases causing a slower charge accumulation process. This was proven in the previous chapter when comparing the results for different contact areas between spherical particles and the ground: decreased contact areas resulted in high contact resistances and therefore slower charging processes. In this section, a direct relation with the mesh pattern was shown, and a conclusion can be deducted: a finite contact area with the ground should be chosen for the particle instead of a point contact, because the point contact is identified by COMSOL upon discretizing the domain as an unknown finite contact area, depending on the size of the discretizations used.

4.8 Summary

To investigate the dynamics of induction charging for spherical particles made out of real conductors in different particle arrangements, and assuming finite volume and surface conductivities, a few different models have been tested. Simulations were conducted using the COMSOL Transient Analysis model in three-dimensional space. Surface layers of the particles were modelled using an equivalent approximation instead of a finite thickness model as done before. This was useful in achieving very thin surface layers. Firstly, the validity and accuracy of a single spherical particle was confirmed by comparing the results to the previously verified two-dimensional models. Following this, it was possible to investigate multiple particle agglomerations in different configurations. The conclusions can be summarized as follows:

For a spherical particle with $\sigma_2 > \sigma_1$, accumulation of charge was slower when decreasing the thickness of the surface layer. Comparing a very thin surface layer to previous 1% and 4.27% surface layer thicknesses, it was shown that τ_c would increase when decreasing the thickness of the layer i.e. a slower charge build up. This can be explained by the effect of surface conductivity, which is directly proportional to surface layer thickness and outer volume conductivity where $\sigma_s = \sigma_2 d$. Therefore, decreasing the surface conductivity would result in a slower charging process for the particles.

Adjusting the parameters of the surface layer to represent actual applications, a surface layer of 20 Å thickness was introduced. Practical conductivity values were chosen. The results of the simulations showed a fast charging process in the milliseconds when compared to previous results in the tens of seconds range. This was due to a high surface conductivity of the particle.

After selecting the parameters of the surface layer, multiple particle agglomerations in various patterns were investigated. A thirteen-particle pattern aligned horizontally was modelled at first. For all shielded particles, the saturation charge decreased as compared with a single unshielded particle. The strongest shielding effect can be observed for a central sphere that had the smallest saturation charge. Electric shielding would result from the close proximity of the particles, blocking mostly the electric field from the lower part of the particles. For a single layer configuration, the presence of adjacent particles reduces the electric field both on the upper and even more on the lower hemi-sphere. The upper hemisphere of the spherical particle would have a

higher charge accumulation than the lower hemisphere and therefore the total charge accumulation would be smaller than that of an unshielded particle.

To further study the effect of electric shielding on the saturation charge, and charging dynamics, a two-layer particle pattern was also created, using a five-over-five particle arrangement. Results showed that the elevated particles in the top layer had higher saturation charge because they are exposed to a stronger electric field, and charges are transferred from the shielded particles to the elevated ones. As before, accumulation of charge was faster for particles with less shielding. For those particles in contact with the grounded electrode, the charging is not monotonic. Firstly, a fast accumulation of charge was noticed; then the total charge decreased. The electric current flows from the ground electrode to the upper particle layer and as it passed through the lower particle layer, transient accumulation of charge occurs. Moreover, not all the electric field would be shielded from the lower particles and, therefore, a small accumulation of charge can be noticed. It was noticed that the central particle in the lower layer is shielded from all sides and had lost most charge upon saturation. This shows the effect of shielding and complies with theoretical interpretations.

Various models were constructed to calculate the saturation charge of the central particle in multi-particle configurations. The particles were aligned horizontally with no shielding from the upper layer. Agglomerations with increasing number of particles were compared (five, thirteen and twenty-one particle patterns). The results showed that saturation charge for a central sphere would decrease upon adding more surrounding

particles, but up to a certain point where adding more particles would have little or no effect on the saturation charge or the actual charging time constant of the central particle.

The discharging process was also simulated. The results obtained from COMSOL simulation showed an excellent agreement with theoretical prediction: both the actual charging and discharging time constants were equal for the particles in all the cases modelled.

Finally, it was of interest to investigate the effect of the mesh pattern. As COMSOL would create finite elements at the contact areas, a point contact would be equivalent to a small finite surface area. Spherical particles having a point contact with the ground were simulated with varying mesh patterns. When a coarse mesh pattern was created, the equivalent contact area with the ground increased and a faster charging process was observed. As verified previously, a larger contact area resulted in smaller contact resistance with the ground and, therefore, a faster charging process. The coarse mesh for a point contact model resulted in a larger equivalent contact area than that of a fine mesh pattern. This resulted in a faster charging process for a coarse mesh. The results proved that a finite contact area should be considered for modelling instead of a point contact as the actual charging time constant is directly affected by the contact area of the particle with the ground.

Chapter 5
Conclusions and Suggestions for Future Work

5.1 Conclusions

In this thesis, the dynamics of induction charging for spherical particles were investigated. Particles with finite surface and volume conductivities, and arbitrary permittivity were simulated in the COMSOL commercial software using the Finite Element Method. Firstly, a single spherical particle exposed to a uniform electric field was modelled in two-dimensional space. The validity of the model was verified by comparing the numerical simulation results with Felici's analytical formulae [2] for regular shaped particles. The actual charging time constant was then compared to the material's relaxation time constant, for different cases of conductivity, permittivity, particle's contact resistance with ground and surface layer thickness. The model was then extended in three-dimensional space to include multiple spherical particles stacked in different particle agglomerations. Surface conductivity was specified as an Electric Shielding boundary condition in COMSOL, instead of assuming a finite thickness of the surface layer, to overcome geometric limitations of this software. The particle's saturation charge, actual charging time constant and charging dynamics were compared for different patterns of particle agglomerations. The results can be summarized as follows:

For the single spherical particle with finite surface layer thickness:

1. Validity of the model was tested by comparing numerical results (saturation charge) for regularly shaped particles (sphere and hemisphere) with Felici's analytical formulae [2]. The results of comparison showed 0.29% error for sphere, and -0.0001% error for hemisphere. Excellent agreement between numerical and analytical results can be concluded.

2. The spherical particle model with increasing contact areas was simulated. The results showed that increasing the contact area between the particle and the grounded electrode (less contact resistance) would significantly shorten the charging time. Charge accumulation on the particle's surface was fastest for a hemisphere having the largest contact area; slowest for a particle with theoretically point contact, having actually finite, but smallest contact area. It was shown that even for a small material relaxation time constant, the actual charging time constant can be significantly large for particles with small contact areas (high contact resistance).

3. For a small finite contact area of 0.039mm^2 with the grounded electrode, and fixed permittivity; outer conductivity σ_2 for the surface area, and inner conductivity σ_1 for the particle were varied. When $\sigma_2 > \sigma_1$, charge accumulation on the particle's surface was faster. Increasing σ_2 implied an increase in surface conductivity ($\sigma_s = \sigma_2 d$), while keeping the surface layer thickness d constant. The results showed a faster charging time for a high surface conductive layer.

4. For the same case of varying the conductivities, increasing the particle's permittivity (ε_1) showed a faster charging time. However, the effect of increasing permittivity was negligible when compared to increasing either of the surface or volume conductivities. The results showed that even for an increased permittivity, particles with less conductive surface layers had a slow charging process. Therefore, it was concluded that the particle's volume or surface conductivity had a more significant effect on the actual charging time constant than its permittivity.

5. For a small finite contact area of 0.039mm^2 with the grounded electrode and fixed permittivity, the ratio of outer to inner conductivity (σ_2/σ_1) and surface layer thickness (d) were varied. For ($\sigma_2/\sigma_1 > 1$), decreasing the surface layer thickness from 10% to 1% showed a slower charging time for the particle. In contrast, for $\sigma_2/\sigma_1 < 1$, decreasing the surface layer thickness from 10% to 1% showed a faster charging process, although to a less extent, due to a high inner conductivity. It was concluded that particles with thick surface layers would accumulate charge faster, a result of high surface conductivity.

6. A discharging simulation for the spherical particle exposed to a uniform electric field was performed. Regardless of conductivity, permittivity, contact area and surface conductivity, the results showed that the actual charging and discharging time constants were equal, yet different from the material's relaxation time constant. A conclusion can be formulated that the actual time constant (charging and discharging) are geometry related and directly dependent on the particle's

surface and volume conductivities; unlike the analytical relaxation time which is dependent only on the bulk material's properties ($\tau_r = \varepsilon_1/\sigma_1$).

For the single spherical particle assuming surface conductivity as a boundary parameter (Electric Shielding) with defined thickness, conductivity and permittivity and fixed finite contact area (using three-dimensional modelling), the following can be concluded:

1. Validity of the new three-dimensional model was tested, and the results compared with previously verified results of the two-dimensional model. The comparison showed 0.001% error for saturation charge and almost identical charging curves. Excellent agreement with previous results was concluded.

2. Decreasing the surface layer thickness below 1% keeping fixed conductivity values showed a slower charging process. The conclusion was the same as before: decreasing the surface layer thickness would make the charging time slower.

3. The spherical particle was then simulated with practical values of surface layer thickness and conductivity. Assuming a higher surface conductivity with very thin surface layer thickness (20 Å), the charging process was much faster than previous cases of finite surface layers 10%, 4.27% and 1%. Even though the 20 Å surface layer was very thin, a very high outer conductivity of the surface layer (0.005 S/m compared to previous cases of 10^{-9} S/m) resulted in a much higher surface conductivity, and, therefore, a faster charging process than the previous cases.

For multiple particle agglomerations with constant surface and volume conductivities, permittivity, and contact area the results can be summarized as follows:

4. In the thirteen-particle agglomeration, particles that are closely surrounded by other particles, experience more shielding of the electric field. The results showed a decreased saturation charge for the shielded particles, and a decreased charging time as less charge would be accumulated

5. In the five-over-five particle pattern, elevated particles showed a high saturation charge and lower shielded particles lost charge in favour of the upper particles. It was concluded that a close proximity of particles for a given particle would significantly decrease its saturation charge.

6. When the number of particles was increased from five to thirteen, a significant decrease in saturation charge was observed for the central particle in the pattern. The number of particles in agglomeration was then increased from thirteen to twenty-one particles; a negligible decrease in saturation charge for the central particle was noticed upon the second increase. It was concluded that shielding the electric field by adding more surrounding particles would decrease the central particle's saturation charge up to a point where adding more surrounding particles would have no further effect on its charging dynamics or maximum induced charge.

7. Discharging for the multiple particle agglomeration showed that the actual charging and discharging time constants are equal.

8. Finally, the effect of a spherical particle's point contact with the grounded electrode was shown, for different mesh patterns simulated in two-dimensional space. A coarse mesh pattern created large elements causing larger equivalent contact area instead of its theoretical point contact; a refined mesh created smaller elements. For larger elements, faster charging time was shown due to less contact resistance. It was concluded that a theoretical point contact cannot be created in COMSOL, because it would result in having an unknown finite contact area with the ground depending on the discretization mesh pattern used. Therefore, choosing a small finite contact area would be the best approach, as simulated in all previous cases.

5.2 Suggestions for Future Work

A few suggestions can be advised for future work:

The simulation model, using COMSOL's "electric shielding" boundary condition was used to simulate negligibly thin surface layer thicknesses and practical surface conductivity values for regularly shaped particles; the spherical particle in this thesis. In practical applications, not only are the particles stacked in arbitrary configurations, but also have irregular shapes. Irregularly shaped particles, having multiple contact areas with the grounded electrode, can be simulated using the surface layer model advised in this thesis. Therefore, analysis would also include particle shape, and multiple contact areas to study their effect on the actual charging time and maximum induced charged.

It was shown that the actual charging time constant relies directly on the particle's geometry and conductivity, and is not related to the analytical relaxation time constant. A quantitative relationship is still to be investigated.

Finally, charging and discharging simulation models can further be investigated for particles having initial space charge density exposed to a non-uniform electric field.

References

[1] W. H. Hayt and J. A. Buck, "*Engineering Electromagnetics*", Seventh Edition, Ohio: McGraw Hill 2002.

[2] N. J. Félici, "Forces et charges de petits objets en contact avec une électrode affectée d'un champ électrique." *Rev. Gén. Elect.*, vol. 75, pp. 1145-60, Oct. 1966.

[3] N. N. Lebedev and I. P. Skal'skaya, "Force acting on a conducting sphere in the field of a parallel plate condenser," *Soviet Phys. Tech. Phys.*, vol. 7, pp. 268-271, 1962.

[4] D. Yu, "Static and dynamic models for induction charging of smooth and rough particles," M.E.Sc. Thesis, The University of Western Ontario, London, Ontario, Canada, 2007.

[5] Y.Wu, G. S. P. Castle, I. Inculet, "Induction charging of granular materials in an electric field," *IEEE Trans. Ind. Appl.*, vol. 4, pp. 2366-2372, Sept./Oct. 2004.

[6] Y. Wu, I. I. Inculet, S. Petigny, G. S. Swei, "Induction charge on freely levitating particles," *IEEE Trans. Ind. Appl.*, vol. 40, pp. 1498-1503, Nov./Dec. 2004.

[7] C. Changrag, K. Asano, K. Yatsuzuka, "The behavior of spherical particle under uniform electric field in silicone oil," *IEEE Trans. Ind. Appl.*, vol. 1, pp. 77-80, Oct. 2000.

[8] L. Dascalescu, P. Ribardière, M. Mihailescu and P. Levin, "Numerical analysis of induction charging of conductive cylinders in non-uniform electric fields," *J. Electrostatics*, vol. 51-52, pp. 597-602, May 2001.

[9] I. I. Inculet and G. S. P. Castle, "Induction charging of flat sprays for space charge generation," *IEEE Trans. Ind. Appl.*, vol. 3, pp. 1946-1949, Sep./Oct. 2001.

[10] K. Adamiak, "Numerical simulation of charge relaxation in low-conductivity fluids stored in cylindrical tanks," *IEEE Trans. Ind. Appl.*, vol. 40, pp. 710-713, Mar. 2004.

[11] R. J. Pazda and T. B. Jones, "Effect of surface conduction on charge relaxation in partially filled vessels," *J. Electrostatics*, vol. 28, pp. 175-185, July 1992.

[12] R. J. Pazda, T. B. Jones and Y. Matsubara, "General theory for transient charge relaxation in a partially filled vessel," *J. Electrostatics*, vol. 32, pp. 215-231, April 1994.

[13] Y. Matsubara, R. J. Pazda and T. B. Jones, "Effect of fill pipe on transient decay of surface potential in a cylindrical vessel containing charged liquid," *IEEE Trans. Ind. Appl.*, vol. 30, pp. 205-209, Jan./Feb. 1994.

[14] K. Robinson, "Charge relaxation due to surface conduction on an insulating sheet near a grounded conducting plane," *IEEE Trans. Ind. Appl.*, vol. 1, pp. 589-598, Oct. 2002.

[15] K. Adamiak, "Rate of charging of spherical particles by monopolar ions in electric fields," *IEEE Trans. Ind. Appl.*, vol. 38, pp. 1001-1008, Jul./Aug. 2002.

[16] L.Dascalescu, D. Rafiroiu, A. Samuila, R. Tobazeon, "Charging of insulating spheres on the surface of an electrode affected by monopolar ions," *IEEE Trans. Ind. Appl.*, vol. 34, pp. 35-42, Jan./Feb. 1998.

[17] J. W. Nilsson and S. A. Riedel, *"Electric Circuits"*, Sixth edition, CA: Prentice-Hall 2000.

[18] J.M. Crowley, *"Fundamentals of Applied Electrostatics"*, Morgan Hill, CA: Laplacian Press, 1999.

[19] R.D. Cook, D.S. Malkus, and M. E. Plesha, *"Concepts and Applications of Finite Element Analysis"*, 2nd Edition, New York: John Wiley and Sons 1982.

[20] *FEMLAB User's Guide*, COMSOL, Stockholm, Sweden, 2004.

[21] ESD Association Advisory, *"Electrostatic Discharge Standards"*, New York, October 2003.

[22] R. Sharma, A.S. Biris, R.A. Sims, M.K. Mazumder, "Effect of ambient relative humidity on charge decay properties of polymer powder and on the occurrence of back corona in powder coating," *IEEE Trans. Ind. Appl.*, vol. 3, pp. 1961-1965, Sep./Oct. 2001.

[23] Intertek Plastics Technology Laboratories *"ASTM D257 IEC60093 Surface and Volume Resistivity Test Method"*, MA, 1998.